SRI International

AD-A222 560

Final Report • January1990

DETECTION OF VIBRATIONALLY EXCITED $H_2(v'')$ FOR H^- PRODUCTION

William K. Bischel, Principal Investigator
R. C. Robie, Research Associate
James R. Peterson, Project Supervisor

SRI Project PYU-2599
MP 89-183

Prepared for:

Air Force Office of Scientific Research
AFOSR/NP
Bolling Air Force Base
Washington, DC 20332-6448

Attention: Lt. Col. Bruce L. Smith, Program Manager
Physical and Geophysical Sciences Directorate

Contract Nc. F49620-86-C-0112

333 Ravenswood Avenue • Menlo Park, CA 94025-3493 • (415) 326-6200 • FAX: (415) 326-5512 • Telex: 334486

UNCLASSIFIED
SECURITY CLASSIFICATION OF THIS PAGE

REPORT DOCUMENTATION PAGE

Form Approved
OMB No. 0704-0188

1a. REPORT SECURITY CLASSIFICATION UNCLASSIFIED	1b. RESTRICTIVE MARKINGS NONE
2a. SECURITY CLASSIFICATION AUTHORITY N/A	3. DISTRIBUTION / AVAILABILITY OF REPORT Approved for public release; distribution unlimited.
2b. DECLASSIFICATION / DOWNGRADING SCHEDULE N/A	
4. PERFORMING ORGANIZATION REPORT NUMBER(S) MP 89-183	5. MONITORING ORGANIZATION REPORT NUMBER(S) AFOSR-TR- 90 0533
6a. NAME OF PERFORMING ORGANIZATION SRI INTERNATIONAL	6b. OFFICE SYMBOL (If applicable)
6c. ADDRESS (City, State, and ZIP Code) 333 RAVENSWOOD AVENUE MENLO PARK, CA 94025-3493	7a. NAME OF MONITORING ORGANIZATION Same as 8a 7b. ADDRESS (City, State, and ZIP Code) Same as 8c
8a. NAME OF FUNDING / SPONSORING ORGANIZATION AFOSR	8b. OFFICE SYMBOL (If applicable) NP
8c. ADDRESS (City, State, and ZIP Code) Bolling Air Force Base Washington, DC 02332-6448	9 PROCUREMENT INSTRUMENT IDENTIFICATION NUMBER F49620-86-C-0112
	10. SOURCE OF FUNDING NUMBERS PROGRAM ELEMENT NO. 61102F; PROJECT NO. 8120; TASK NO. G1; WORK UNIT ACCESSION NO.

11. TITLE (Include Security Classification)
Detection of Vibrationally Excited $H_2(v'')$ for H Production

12. PERSONAL AUTHOR(S)
William K. Bischel, Daniel C. Robie, and James R. Peterson

13a. TYPE OF REPORT	13b. TIME COVERED	14. DATE OF REPORT (Year, Month, Day)	15. PAGE COUNT
Final	FROM 860901 TO 890831	890915	65

16. SUPPLEMENTARY NOTATION

17. COSATI CODES		
FIELD	GROUP	SUB-GROUP
7	2	
20	5	

18. SUBJECT TERMS (Continue on reverse if necessary and identify by block number)
Multiphoton Ionization of H_2, (H_2^-) Source Development, Photoabsorption Techniques, Stimulated Emission, Laser-induced Fluorescence (JES)

19. ABSTRACT (Continue on reverse if necessary and identify by block number)

Research was performed to develop laser-based detection of high-lying vibrational levels ($v = 4$-10) of H_2 to aid the development of high intensity H^- ion production from H_2 plasmas. A new type source of vibrationally excited H_2 was developed, and a 2-photon resonantly enhanced multiphoton ionization (REMPI) was developed and was successful in detecting $H_2(v)$ in levels up to $v = 11$. A technique was developed for measuring the tuning range and bandwidth of a tunable ArF laser used to generate vacuum-ultraviolet photons. Two-photon absorption cross sections for $X \rightarrow EF$ excitation in H_2 were calculated for a wide range of X and EF vibrational levels. Attempts to use both one- and two-photon laser-induced fluorescence to detect excited levels were unsuccessful.

20. DISTRIBUTION / AVAILABILITY OF ABSTRACT	21. ABSTRACT SECURITY CLASSIFICATION
☒ UNCLASSIFIED/UNLIMITED ☐ SAME AS RPT ☐ OTIC USERS	Unclassified
22a. NAME OF RESPONSIBLE INDIVIDUAL Lt. Col. Bruce L. Smith	22b TELEPHONE (Include Area Code) (202) 767-4908
	22c OFFICE SYMBOL NP

DD Form 1473, JUN 86 Previous editions are obsolete. SECURITY CLASSIFICATION OF THIS PAGE

UNCLASSIFIED

CONTENTS

RESEARCH OBJECTIVES

A major effort has been under way for some years to develop high-intensity, high-energy neutral beams of H atoms, which are made by the neutralization of negative ion beams. H^- ion beam sources are well known, but the ion production mechanism is poorly understood.

The goal of this research has been to develop nonintrusive methods for detecting high-lying vibrational levels ($v > 4$) of H_2 that are considered essential to the efficient operation of H^- in "volume production" ion sources. These ion sources are in turn essential to the development of high-intensity, high-brightness beams of neutral H atoms at high energies (250 keV to 2 MeV) for use in heating tokamak plasmas in fusion energy devices and for neutral particle beam directed-energy weapons. Although a great deal of progress has been made in the development of these ion sources, the actual mechanisms responsible for their efficiency (and thus for further improvements) are not well understood. It is believed that the main source of H^- is dissociative attachment of electrons to highly vibrationally excited H_2 in its ground electronic state. However, the populations of these vibrational levels, which are the central quantities of models of these sources, had not been measured *in situ* when this project began.

We proposed to develop laser-based detection methods for determining, with high spatial resolution, the populations of the relevant levels, especially those above $v = 4$-10. The techniques we investigated include two-photon resonantly enhanced multiphoton ionization (REMPI), one-photon laser-induced fluorescence (LIF) via the electronically excited B state, and two-photon LIF via the excited EF state. We pursued this objective on two fronts. First, we developed techniques for generating and characterizing tunable vacuum ultraviolet (VUV) laser radiation, including a new method for measuring the bandwidth of an ArF excimer laser and Raman-shifting that laser into the VUV. Second, on the basis of recent breakthroughs in Europe, we built and characterized a new type of source for highly vibrationally excited ground state H_2. Using this source and our two-photon REMPI system, we demonstrated production of H_2 in vibrational levels up to $v = 11$.

ACCOMPLISHMENTS

The main objective of this project was to develop portable methods for measuring *in situ* the population of vibrational levels of H_2 with high spatial resolution inside plasmas. The requirements of sensitivity and spatial resolution suggested laser-based techniques, and we investigated two: laser-induced fluorescence (LIF), both one- and two-photon, and two-photon resonantly enhanced multiphoton ionization (REMPI).

We measured precisely the two-photon absorption cross section for H_2 from the $X\ ^2\Sigma(v'' = 0, J'' = 1)$ state to the $EF\ ^2\Sigma(v' = 6, J'' = 1)$ state. This measurement substantially resolved outstanding discrepancies between theory and previous experiments. It was published in *Physical Review* in 1989, and appears here as Appendix A.

We developed a technique based on 1 + 1 REMPI of NO, for measuring the tuning range and bandwidth of a tunable ArF excimer laser used for generating VUV photons. This technique has been described in a paper accepted for publication in *Applied Optics*, entitled "Bandwidth and Tuning Range of an ArF Laser Measured by 1 + 1 Resonantly Enhanced Multiphoton Ionization of NO," which is attached as Appendix B.

We used a 2 + 1 REMPI method to sample the vibrational population and were able to detect populations in vibrational levels up to $v = 11$, currently the highest vibrational level of H_2 ever observed by photoabsorption techniques. The work has been described in a paper submitted for publication in *Applied Physics Letters* and entitled "Generation of Highly Vibrationally Excited H_2 and Detection by 2 + 1 Resonantly Enhanced Multiphoton Ionization;" it is attached as Appendix C.

On the basis of our success in measuring the two-photon cross section for the $X \rightarrow EF$ transition in H_2, new cross sections for two-photon excitation in $EF \leftarrow X$ bands were performed under this contract by a consultant, Dr. Winifred Huo of NASA-Ames. These calculations, are discussed in Appendix D and will be incorporated in a manuscript to be submitted to *Physical Review A*.

We performed exploratory experiments discussed in Appendix E, using a new stimulated-emission technique for generating H_2 (X, $v = 6$-9). We believe this technique holds great promise for further work on the dynamics of highly vibrationally excited H_2.

We investigated two-photon LIF in H_2, delineating the problems in that method, and constructed a Raman-shifted ArF excimer source of tunable VUV light. With this source, we demonstrated anti-Stokes Raman shifting in H_2 and D_2 up to the fourth order and began a search for one-photon LIF in H_2 but were still unsuccessful at the conclusion of this contract.

PUBLICATIONS AND CONFERENCE PRESENTATIONS

The following papers and conference presentations were produced under this contract.

1. J. D. Buck, D. C. Robie, A. P. Hickman, D. J. Bamford, and W. K. Bischel, "Two-Photon Excitation and Excited-State Absorption Cross Sections for H_2 E_1 F^1 Σg (v = 6): Measurement and Calculations," Phys. Rev. A **39**, 3932 (1989). A reprint of this paper is included as Appendix A.

2. D. C. Robie, J. D. Buck, and W. K. Bischel, "Bandwidth and Tuning Range of an ArF Laser Measured by 1 + 1 Resonantly Enhanced Multiphoton Ionization of NO," submitted for publication in Applied Optics. A copy of this paper is included as Appendix B.

3. D. C. Robie, L. E. Jusinski, and W. K. Bischel, "Generation of Highly Vibrationally Excited H_2 and Detection by 2 + 1 Resonantly Enhanced Multiphoton Ionization," submitted for publication in Applied Physics Letters. A copy of this paper is included as Appendix C.

4. D. C. Robie, L. E. Jusinski, and W. K. Bischel, "Laser-Based Detection of Highly Vibrationally Excited H_2 for Plasma Diagnostics," poster presented at the Forty-first Annual Gaseous Electronics Conference, Minneapolis, October 18, 1988, and at the 1988 annual meeting of the Optical Society of America, Santa Clara, California, November 1, 1988, and published in Proc. SPIE **1061**, 617-619 (1989). A reprint of this paper is included as Appendix F.

5. W. K. Bischel, D. C. Robie, and J. D. Buck, "Two-Photon Ionization of NO at 193 nm for ArF Laser Diagnostics," poster presented at the Third International Laser Science Conference, Atlantic City, New Jersey, November 2, 1987.

6. D. C. Robie, L. E. Jusinski, and W. K. Bischel, "Laser-Based Detection of Highly Vibrationally Excited H_2 for Plasma Diagnostics," paper presented at a meeting of the Society of Photo-Optical Instrumentation Engineers (SPIE), Los Angeles, January 15, 1989.

7. D. C. Robie, L. E. Jusinski, and W. K. Bischel, "Generation of H_2 (v = 4-11) and Its Laser Spectroscopy," paper presented at the First Quantum Electronics and Laser Science Conference, Baltimore, April 26, 1989.

8. D. C. Robie, M. J. Dyer, L. E. Jusinski, W. K. Bischel, and W. Huo, "Photodiagnostics of Vibrationally Excited H_2 Using 2 + 1 Multiphoton Ionization Through the EF State," to be submitted, 1990.

PROFESSIONAL PERSONNEL

The following professional personnel contributed to the project:

Dr. William K. Bischel, Project Leader

Dr. James R. Peterson, Project Supervisor

Dr. David R. Crosley

Dr. Daniel C. Robie, Postdoctoral Fellow

Dr. Jesse D. Buck, Postdoctoral Fellow

Appendix A

TWO-PHOTON EXCITATION AND EXCITED-STATE ABSORPTION CROSS SECTIONS FOR H_2 E, F $^1\Sigma_g$ (v = 6): MEASUREMENT AND CALCULATIONS

Two-photon excitation and excited-state absorption cross sections for H_2 $E,F\ ^1\Sigma_g^+$ ($v=6$): Measurement and calculations

Jesse D. Buck,* Daniel C. Robie, A. P. Hickman,
Douglas J. Bamford,† and William K. Bischel
Molecular Physics Laboratory, SRI International, Menlo Park, California 94025
(Received 21 November 1988)

The absolute two-photon excitation cross section for the H_2 $E,F\ ^1\Sigma_g^+$ ($v'=6$)←$X\ ^1\Sigma_g^+$ ($v''=0$) $Q(1)$ transition at 193 nm has been measured by observing the $E,F\ ^1\Sigma_g^+$ ($v'=6$)→$B\ ^1\Sigma_u^+$ ($v''=0$) fluorescence at ~750 nm. The measured integrated two-photon excitation cross section, $(2.0\pm0.9)\times10^{-36}$ cm^4, is in good agreement with the theoretical value of 2.8×10^{-36} cm^4, which is obtained from previously published calculations [Huo and Jaffe, Chem. Phys. Lett. **101**, 463 (1983)]. The absolute cross section for photoabsorption by the E,F state at 355 and 193 nm was also measured by monitoring the depletion of the 750-nm fluorescence caused by a second laser. The measured cross sections for photoabsorption by the E,F ($v=6$) state are $(9.7\pm2.4)\times10^{-18}$ cm^2 at 355 nm and $(6.4\pm1.3)\times10^{-18}$ cm^2 at 193 nm. Comparison with theoretical estimates [Cohn, J. Chem. Phys. **57**, 2456 (1972)] of the direct photoionization cross section of this state (8.5×10^{-18} cm^2 at 355 nm and 3.2×10^{-18} cm^2 at 193 nm) suggests that other processes may contribute to the photoabsorption. Photoexcitation of the dissociating $^1\Sigma_u$ autoionizing state is found to be important. Cross sections for this additional channel, which may lead to dissociation (H^*+H or H^++H^-) or autoionization ($H_2^++e^-$), are calculated to be 3.6×10^{-18} cm^2 at 355 nm and 7.6×10^{-18} cm^2 at 193 nm. The calculated branching ratio strongly favors dissociation at 355 nm and autoionization at 193 nm.

I. INTRODUCTION

Molecular hydrogen occupies a position of unique importance in chemical physics because it is the simplest neutral molecule. As such, it supports a rich interplay between experiment and theory, due largely to the relative tractability of large-scale calculations on this four-particle molecular system. Hydrogen is also of considerable practical importance in areas such as combustion,[1] extraterrestrial atmospheres,[2] vacuum-uv laser sources,[3] laser-based analytical probes,[4] and numerous others. In view of this, we have undertaken a series of experiments to compare absolute cross-section measurements to calculations for two-photon resonant multiphoton transitions in H_2. *Ab initio* calculations of the two-photon transition moment[5] for H_2 E,F ($v'=6$)←X ($v''=0$) have been available in the literature for several years and can be used to compare to quantitative measurements. In addition, this research was motivated by the need to develop detection methods for vibrationally excited ground electronic state hydrogen for application to the diagnostics of H^- plasma sources.[6,7] We expect the results reported here for the $v''=0$ ground vibrational state will serve as a benchmark for determining the sensitivity for H_2 ($v''>0$) detection using two-photon excitation.

In this paper we report absolute measurements of both the two-photon cross section for excitation in the transition from the X ($v''=0$) to the E,F ($v'=6$) state of H_2, and cross sections for absorption by the excited state. The wavelength dependence of the absorption cross section σ_{abs} is of particular interest since several mechanisms in addition to direct photoionization can contrib-

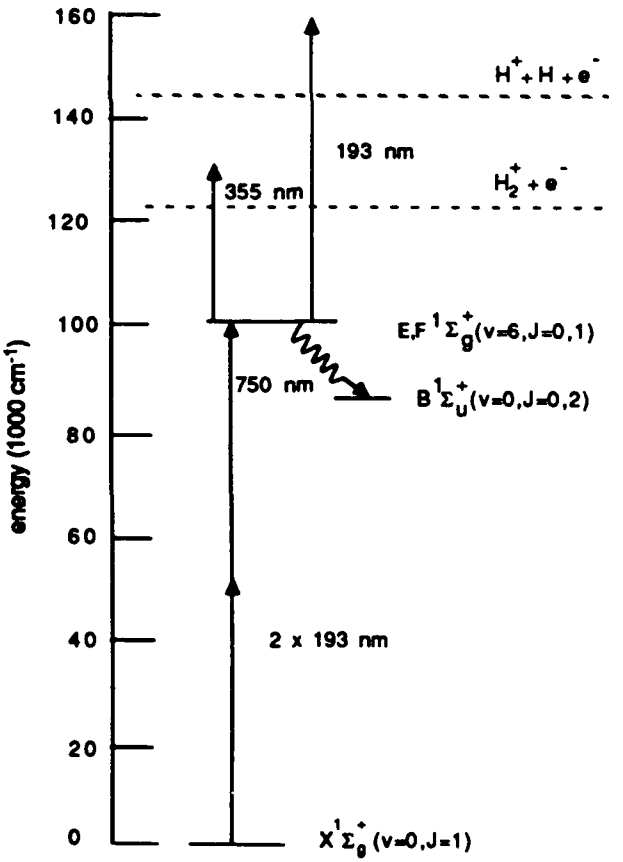

FIG. 1. Selected energy levels for H_2. The threshold for ionization is 124 417 cm^{-1}; for dissociative ionization the threshold is 145 796 cm^{-1} (Ref. 35).

ute.[8-10] As a first experiment in this direction, we have measured the total absorption cross section at two wavelengths (193 and 355 nm). These results are compared to theoretical calculations of the cross sections for direct photoionization and for other channels contributing to absorption.

The H_2 energy levels relevant to the work reported here are given in Fig. 1. The $J'=1$ rotational level of the E,F ($v'=6$) level was excited using two-photon absorption at 193 nm. The excited level either fluoresced in the near-ir region (750–840 nm) or absorbed a third photon (either at 193 or 355 nm). The experiment consisted of quantitatively measuring either the fluorescence produced in the two-photon process or the depletion of fluorescence caused by absorption of a third photon, and measuring the laser intensity in the observation volume. Using techniques previously developed in this laboratory,[11,12] two-photon excitation cross sections were derived from the data. Using the fluorescence depletion technique,[13] excited-state absorption cross sections were also obtained.

The paper is organized as follows. Section II describes the experiment, including a detailed description of two methods used to produce tunable radiation at 193 nm. Section III describes the theoretical calculations. Two-photon excitation cross sections for the $E,F \leftarrow X$ transition, and for the direct photoionization of the E,F state, are derived from work already in the literature. Photoexcitation to a dissociating, autoionizing $^1\Sigma_u$ state from the E,F state is treated. Section IV compares and discusses the experimental and theoretical results, and Sec. V presents concluding remarks.

II. EXPERIMENT

A. Apparatus and procedure

The apparatus, methods of data acquisition, and analysis used here for the two-photon absorption cross-section measurements have been previously described in detail for atomic oxygen.[12] The apparatus is diagramed in Fig. 2. Tunable laser radiation at 193 nm was generated using two different methods. This allowed the comparison of cross-section measurements using coherent sources that had significantly different photon statistics, bandwidths, and spatial temporal characteristics. In the first method a frequency-doubled Nd:yttrium-aluminum-garnet (YAG)-pumped dye laser (Quanta-Ray DCR2+PDL) was Raman shifted in H_2 to generate over 100 μJ in the fourth anti-Stokes (AS) order at 193 nm. Because the first Stokes order of the Raman-shifted dye laser fundamental has nearly the same wavelength as the fluorescence being observed ($\sim$750 nm), it was necessary to prevent any stray light from the Raman cell from reaching the photomultiplier. This was achieved by focusing the 193-nm beam (fourth AS order) with a 20-cm lens through a small pinhole in an opaque enclosure which surrounded the Raman cell output and the Pellin-Broca prism used to separate the various beams. A second 20-cm lens outside the enclosure then reconverged the 193-nm beam to a focus $\sim$100 cm away in the experimental cell. Pulse energies of up to 50 μJ were focused into the experimental cell. The pulse length was 4 ns, and the fourth AS bandwidth was $\sim 1\ cm^{-1}$.

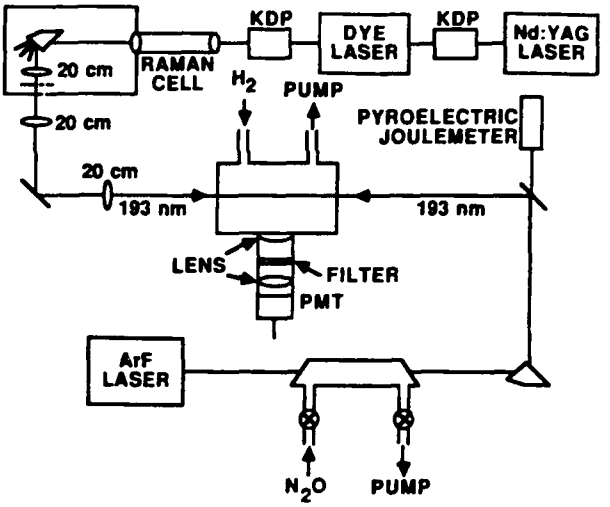

FIG. 2. Apparatus for measurement of the excited-state absorption cross section at 193 nm in H_2. The E,F ($v'=6$)$\leftarrow X$ ($v''=0$) $Q(1)$ two-photon absorption cross section was measured in a similar apparatus, with the ArF laser beam blocked, and the last 20-cm lens removed. To measure the excited-state single-photon absorption cross section at 355 nm, the potassium dihydrogen phosphate (KDP) crystal was used to generate both 532-nm radiation (to pump the dye laser) and 355-nm radiation. The latter follows a path like that of the ArF laser beam.

The second laser source of tunable 193-nm radiation was a commercial two-cavity excimer laser with a grating-tuned oscillator-amplifier system (Lambda Physik EMG150). The beam from the oscillator was amplified with a single pass through the amplifier cavity to an energy of 1–2 mJ/pulse, with a pulse width of 12 ns and a bandwidth of 0.3 cm^{-1}. Much higher pulse energies could be obtained by using unstable resonator optics on the amplifier and injection locking it with the oscillator output, and this configuration was used for the two-laser

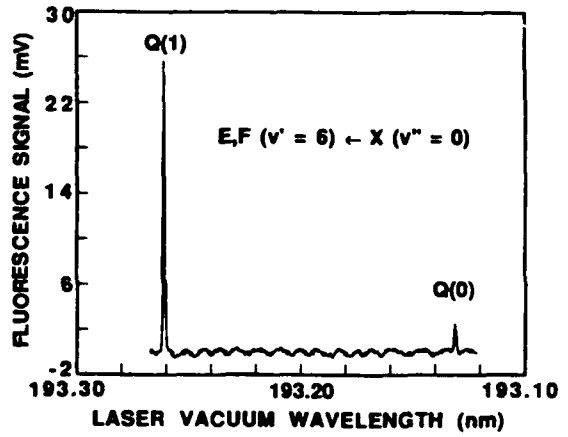

FIG. 3. Fluorescence signal as a function of ArF excimer wavelength. These scans were used to calibrate the wavelength scale.

depletion studies described below. The single-pass configuration eliminated effects from unlocked broadband output on the two-photon absorption measurements, which are sensitive to the laser bandwidth.

The laser energy at 193 nm was varied by admitting 5 mol% N_2O in Ar into a 50-cm-long cell equipped with Brewster windows which the laser beam passed through prior to entering the fluorescence cell. (5 mol% Cl_2 in Ar was used to attenuate the 355-nm beam.) A few hundred Torr of the N_2O mixture was sufficient to extinguish the laser beam, and the attenuation could be continuously varied by pumping out the mixture. The laser energy was measured at the cell exit, with a correction made for the window loss in the single laser experiments.

The wavelength of the excimer laser was calibrated by observing the fluorescence excitation spectrum with both the $E,F\ (v'=6)\leftarrow X\ (v''=0)\ Q(1)$ and $Q(0)$ lines shown in Fig. 1. Typical data for this calibration scan are given in Fig. 3. Additional wavelength calibration experiments were performed using 1+1 two-photon ionization in NO.[14]

Radiation at 355 nm was obtained from frequency tripling for the Nd:YAG laser. This produced 30 mJ in a pulse 5 ns long. The beam had a roughly top-hat spatial profile, but exhibited considerable spatial mode structure.

The experimental cell was equipped with parallel electrodes running the length of the cell for ion detection, and a fast aspheric lens to collect the near-ir fluorescence from the excited molecules due to the transition $E,F\ (v'=6, J'=1)\rightarrow B\ (v''=0, J''=0,2)$. H_2 flowed through the cell at pressures of 0.2–0.3 Torr. We detected a multiphoton ionization signal. However, small quantities of easily ionized impurities in the gas system (presumably vacuum pump oil) interfered with the resonant ionization signal giving a relatively large background signal.

Fluorescence collimated by the aspheric lens and transmitted by a 750-nm bandpass filter was refocused by a second lens (nominal f number ~ 0.7) onto an RCA C31034A photomultiplier tube. The fluorescence signal was integrated with an Ortec 113 preamplifier for all the two-photon absorption measurements. The fluorescence signal was recorded while scanning the laser through the $E,F\ (v'=6)\leftarrow X\ (v''=0)\ Q(1)$ transition at various pulse energies.

The excited-state decay rate was measured by fitting a single exponential to the time-resolved fluorescence signal (acquired on a Tektronix 2430 digital oscilloscope in averaging mode without the Ortec 113 preamplifier). This was used for the total decay rate $\sum_{v''} A_{6v''} + Q$ [see Eq. (1)]. The collisional quenching rate by H_2 was measured to be 1.95×10^{-9} cm^{3}s^{-1}, close to the value previously measured by Kligler and Rhodes.[15]

The spatial beam profile was measured with a pyroelectric detector array which has 100-μm resolution (Spiricon LP-256-11-SP). Scanning a pinhole across the beam gave the same result as the more convenient pyroelectric array. The temporal pulse profiles were measured by reflecting a fraction of the beam onto a fast photodiode (100-ps rise time, Instrument Technology Limited) and observing the output on a 1-GHz oscilloscope (Tektronix 7104). Several pulses were photographed for each run, then digitized by hand. They were subsequently integrated (or squared and integrated) and averaged.

Excited-state absorption cross sections were measured in a pump-probe arrangement in which the fourth AS beam pumped some molecules into the E,F state and either the excimer beam or the tripled Nd:YAG beam depleted a fraction of the excited population after a several nanosecond time delay.[13] The two-laser fluorescence depletion experiments had the advantage that the absolute number density of excited molecules did not need to be known, since the fractional depletion of the lower level in the absorption of the third photon was directly measured. A short focal length ($f=20$ cm) lens was used in the pump laser beam, generating a high density of excited molecules in a small volume which was viewed by the photomultiplier. A significant fraction of the excited molecules absorbed a third pump laser photon. Because the absorption cross-section measurement did not depend on the excited-state density, this did not affect the result. A second laser pulse spatially overlapped the pump laser focus, and was delayed in time by ~ 10 ns. [The excimer laser was tuned to a wavelength near the $E,F\ (v'=6)\leftarrow X\ (v''=0)\ Q(1)$ two-photon transition. No fluorescence could be detected with the pump beam blocked. The wavelength of the excimer laser beam was then within 0.05 nm of 193.26 nm.] In order to be certain that all the excited population was subjected to the same ionizing laser fluence, the time-delayed probe beam was not focused. High pulse energies were then required to produce measurable depletion. By placing a gate on the fluorescence signal ~ 20 ns after the delayed laser pulse had ended, the fluorescence was observed to be depleted by the delayed laser. A second gate was placed at the peak of the fluorescence signal prior to the delayed probe laser pulse; this provided a signal proportional to the density of two-photon excited molecules for shot-to-shot normalization. This signal was unaffected by the probe laser. The ratio (delayed fluorescence signal)/(peak fluorescence signal) at each delayed probe laser power was divided by the value of the ratio with the delayed probe laser absent.

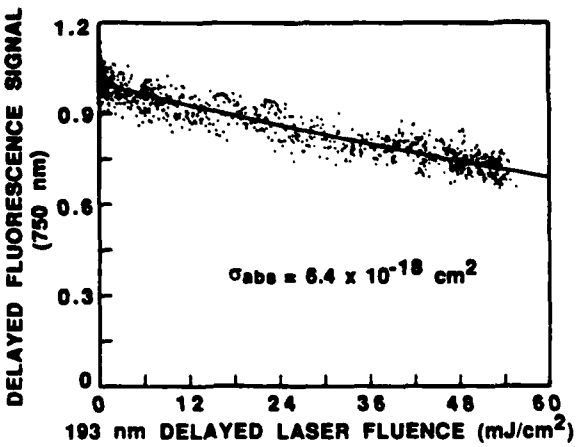

FIG. 4. Fluorescence depletion measurement at 193 nm. The solid curve shows a least-squares fit to an exponential decay.

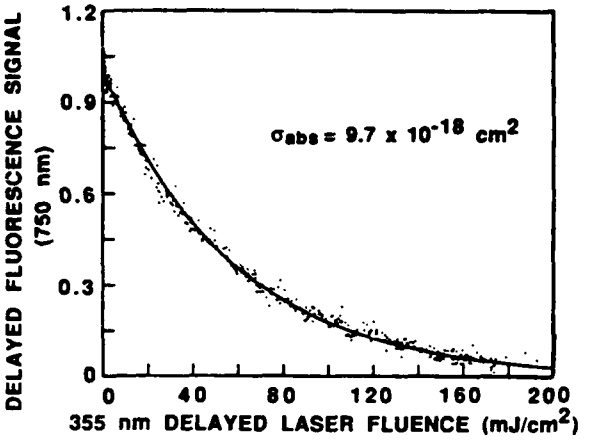

FIG. 5. Fluorescence depletion measurement at 355 nm. The solid curve shows a least-squares fit to an exponential decay.

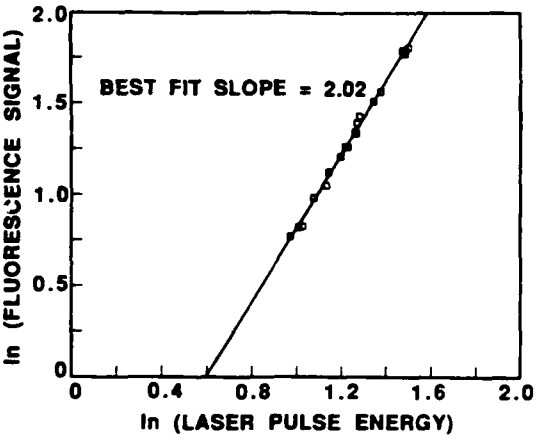

FIG. 6. Intensity dependence of the fluorescence signal for data given in run 2 of Table II.

Because the decay rate of the excited population by fluorescence or collisional quenching was unaffected by the probe laser, this normalization eliminated effects of those processes on the results.

The pulse energy of the delayed laser was varied from zero to full power, and a plot of delayed fluorescence versus delayed laser was recorded. Typical depletion plots are shown in Fig. 4 for 193-nm absorption, and in Fig. 5 for 355-nm absorption. The plots show an exponential decay. The decay constant of the delayed fluorescence as a function of the fluence of the delayed laser (in photons/cm^2) equals the cross section in cm^2 for absorption of a photon from the delayed laser beam. The fluence of the delayed laser was determined by removing the fluorescence cell and placing a 100-μm-diam pinhole at the waist of the focused pump beam, and then measuring the energy of the delayed laser beam which went through the pinhole. Since the delayed laser beam was not focused, the 100-μm pinhole had adequate resolution to measure the laser fluence.

B. Measurements

Plots of ln(peak signal) versus ln(laser energy) for one-laser data were prepared to determine the effective order of nonlinearity, k, where k is the apparent number of photons involved in a given process:

$$k \equiv \partial \ln(\text{signal})/\partial \ln(\text{energy}) .$$

The plot of the fluorescence data had a slope of 2, which is expected for a two-photon process in the absence of saturation (Fig. 6).

An effective two-photon excitation cross section $[\hat{\sigma}^{(2)}(\omega)]$ was calculated using the formula[12]

$$\hat{\sigma}^{(2)}(\omega)=\frac{S(\omega)}{E^2}\frac{\sum_{v''} A_{6v''}+Q}{A_{60}}\frac{4\pi^2 r_0^2(\hbar\omega)^2}{N_0 D\int_{-\infty}^{\infty}F^2(t)dt} , \quad (1)$$

where $\hat{\sigma}^{(2)}(\omega)$ (also known as the two-photon rate coefficient[16]) is the effective two-photon cross section in units of cm^4 s: $S(\omega)/E^2$ is the fluorescence signal in volts divided by the square of the pulse energy: r_0 is the $1/e^2$ radius of the laser beam intensity (fit to a Gaussian profile; averaged over the fluorescence viewing region); $\hbar\omega$ is the energy of a single laser photon; N_0 is the density of molecules in the initial state of the two-photon transition; and D is the calibration constant for the fluorescence detection system.[11] $F(t)$ is the measured temporal laser profile, defined as in Ref. 12:

$$I(r,z,t)=U(r,z)F(t) ,$$
$$\int_{-\infty}^{\infty}F(t)dt=1 ,$$

where $I(r,z,t)$ is the beam intensity and $U(r,z)$ is the fluence. The fluorescence quantum yield is

$$\frac{A_{60}}{\sum_{v''} A_{6v''}+Q} ,$$

where A_{60} is the Einstein A coefficient for the detected fluorescence in the E,F $(v'=6)\rightarrow B$ $(v''=0)$ band, Q is the rate of collisional quenching, and $\sum_{v''} A_{6v''}$ is the sum of Einstein A coefficients for fluorescence in all bands ($\sum_{v''} A_{6v''}=1.01\times10^7$ sec^{-1}). The quantity A_{60} was obtained from a theoretical calculation[17] of the band transition moment (Table I).

The fluorescence detection system was calibrated with spontaneous Raman scattering of a visible laser beam by a static fill of $\sim$1 atm H_2 in the experimental cell to produce a known photon flux at the wavelength of interest.[11] The most important fluorescence wavelengths and calculated branching ratios are listed in Table I. The ratio of the strengths of two rotational lines originating at the same level within a band equals the ratio of the Hönl-London factors for the two lines. We collected photons from two lines only, the $P(2)$ and $R(0)$ lines originating at the E,F $(v'=6, J'=1)$ level and terminating in the B $(v''=0, J''=2,0)$ levels, at wavelengths 752.7 and 746.2 nm, respectively. The ratio of the calculated Hönl-London factors for these two lines in a Σ-Σ transition is 2.[18] The calibration constant D [see Ref. 11, Eq. (1)] was measured in each run at an intermediate wavelength,

TABLE I. Fluorescence wavelengths, Einstein A coefficients, and branching ratios for H_2 E,F ($v'=6, J'=1$).

Lower level	$\lambda[R(0)]$ (nm)	$\lambda[P(2)]$ (nm)	$A_{6v''}$ (s^{-1})[a]	Branching ratio
B ($v''=0$)	746.2	752.7	3.6×10^6	0.36
B ($v''=1$)	827.6	835.2	4.9×10^6	0.49
B ($v''=2$)	925.7	934.9	2.6×10^5	0.03
B ($v''=3$)	1047	1058	2.4×10^4	0.002
B ($v''=4$)	1070	1082	7.7×10^4	0.008
B ($v''=5$)	1396	1415	4.6×10^5	0.05
All others	>1400	>1400	7.3×10^5	0.07
Total			1.01×10^7	1.00

[a]Reference 17.

748.8 nm; then D was measured once at several wavelengths. Combining the ratio of line strengths and the wavelength dependence of the apparatus responsivity, it was found that $D_{\text{eff}}=0.89D_{748.8}$, where $D_{\text{eff}}=\frac{2}{3}D_{752.7}+\frac{1}{3}D_{746.2}$.

The two-photon excitation cross section was measured several times, varying the beam diameter at the focus. The measured parameters for Eq. (1) are listed in Table II for each run. In run 6, a cylindrical beam profile was obtained by sending the collimated laser beam through an aperture just before the fluorescence cell, in which case the radius of the cylindrical profile could be directly substituted for r_0 in Eq. (1). [See the derivation of Eq. (1) in Ref. 12.] Large variations between runs in the photomultiplier calibration constant D were caused primarily by the use of different photomultiplier tube bias voltages to obtain optimum signals for data acquisition.

The two-laser absorption cross-section measurement at 193 nm was performed several times in a two-day period. Successive runs agreed to within about 2%, while all the data agreed to within 10%. We attribute the 10% spread to random error in calibrating the fluence of the delayed laser. An uncertainty of 20% for the fluorescence depletion measurements includes possible systematic errors (mainly pyroelectric detector calibration). We found an excited-state absorption cross section of $(6.4\pm1.3)\times10^{-18}$ cm^2 at 193 nm.

The two-laser absorption cross-section measurement at 355 nm showed a greater run-to-run variation (~15%) than the 193-nm measurement. This was probably due to the pronounced spatial mode structure of the Nd:YAG laser output which makes it more difficult to uniformly irradiate the excited molecule region with the 355-nm laser output. We obtained a value of $(9.7\pm2.4)\times10^{-18}$ cm^2 for the excited-state absorption cross section at 355 nm.

C. Role of photon statistics

The line-shape-independent, two-photon excitation cross section $\sigma_0^{(2)}$, which is a fundamental property of the molecule, is related to the effective cross section defined by Eq. (1) as follows:[16]

$$\hat{\sigma}^{(2)}(\omega)=\sigma_0^{(2)}g(\omega)G^{(2)}, \tag{2}$$

where $g(\omega)$ is the area-normalized line-shape function, and $G^{(2)}$ is the second-order intensity autocorrelation function of the laser,

$$G^{(2)}=\frac{\langle f^2(t)\rangle}{\langle f(t)\rangle^2}, \tag{3}$$

TABLE II. Experimental parameter values for $\sigma_0^{(2)}$ measurement.

Parameter (units)	Run 1	Run 2	Run 3	Run 4	Run 5	Run 6
S/E^2 (10^7 V/J^2)	68.4	7.04	0.395	0.217	0.372	2.42
ω_0^2 (10^{-3} cm^2)	1.81	0.848	2.03	1.57	1.73	3.39
$A_{60}\Big/\left[\sum_{v''}A_{6v''}+Q\right]$	0.114	0.109	0.115	0.114	0.135	0.110
N_0 (10^{15} cm^{-3})[a]	7.15	7.57	7.04	7.08	5.41	7.41
D (10^{-7} V cm sr)	168	15.2	4.94	1.25	2.71	80.5
$\int F^2(t)dt$ (10^8 s^{-1})	3.01	3.00	0.755	0.800	0.772	0.871
$\hat{\sigma}^{(2)}(0)$ (10^{-47} cm^4 s)	1.25	0.660	1.11	1.74	1.76	0.599
$G^{(2)}\sigma_0^{(2)}$ (10^{-36} cm^4)	4.3	2.0	3.6	3.9	5.8	1.3
Laser type	dye	dye	ArF	ArF	ArF	ArF
$G^{(2)}$ (assumed)	1.4	1.4	2.0	2.0	2.0	2.0
$\sigma_0^{(2)}$ (10^{-36} cm^4)	3.1	1.4	1.8	1.9	2.9	0.65

[a]Density in the $J''=1$ rotational level of H_2. The quenching rate Q was calculated using the total density with $N_T=1.52N_0$.

where $f(t)$ is the true area-normalized temporal profile of the laser pulse measured with an infinitely fast detector. The angular brackets denote time averaging over a scale long compared to the coherence time of the laser, but short compared to the laser pulse length:[19]

$$\langle f(t)\rangle = \frac{1}{\Delta t}\int_t^{t+\Delta t} f(t')dt' ,$$

$$\langle f^2(t)\rangle = \frac{1}{\Delta t}\int_t^{t+\Delta t} f^2(t')dt' ,$$

The response time of the photodiode used is in the proper range; thus $\langle f(t)\rangle$ equals the observed $F(t)$. The bandwidth of the excimer laser was considerably smaller than that of the Raman-shifted laser, but the observed linewidths [and hence $g(\omega)$] were mainly determined by the sizable Doppler width for H_2 (0.90 cm^{-1}). The quantity $G^{(2)}\sigma_0^{(2)}$ is obtained in absolute units by integrating $\hat{\sigma}^{(2)}(\omega)$ over the excitation profile, as discussed previously.[12,19]

The factor $G^{(2)}$ characterizes the photon statistics of the pump beam, which must be taken into account when a multiphoton cross section is compared with theory. Our detection apparatus is too slow to capture the intensity variations (on a time scale of ps) of the multimode laser output. The factor $G^{(2)}$ may be thought of as expressing the amount of "spikiness" in the beam intensity that cannot be resolved by the photodiode. This point has been more fully discussed for two-photon excitation in atomic oxygen in Ref. 19.

We used $G^{(2)}=1.4$ for the Raman-shifted dyer laser,[19] and 2.0 for the excimer laser (i.e., the excimer laser was assumed to be a chaotic source). These choices are reasonably consistent with the present results: the average value of $G^{(2)}\sigma_0^{(2)}$ for the Raman-shifted laser measurements (runs 1 and 2) is 3.1×10^{-36} cm^4, while for the excimer laser (runs 3–6) it is 3.7×10^{-36} cm^4. The ratio $3.7/3.1=1.2$, which is fairly close to $2.0/1.4=1.4$. The scatter is too large to consider the difference significant. The average of $G^{(2)}\sigma_0^{(2)}$ from runs 1 and 2 divided by 1.4, and runs 3–6 divided by 2.0, is $\sigma_0^{(2)}=(2.0\pm0.9)\times10^{-36}$ cm^4.

III. THEORY

A. Comparison of $\sigma_0^{(2)}$ with previous calculations

The theoretical value of the integrated two-photon excitation cross section $\sigma_0^{(2)}$ (in cm^4) was obtained from the calculated two-photon transition moment[5] using the formula[16]

$$\sigma_0^{(2)}=(2\pi)^3\left[\frac{e^2}{\hbar c}\right]^2(\hbar\omega)^2P^2 , \tag{4}$$

where

$$P=\sum_k \frac{\langle f|r|k\rangle\langle k|r|g\rangle}{E_g-E_k+\hbar\omega} \tag{5}$$

is the two-photon transition moment for excitation by one laser beam; here g, k, and f refer to the ground, virtual intermediate, and final states of the transition, respectively; r is the dot product of the dipole moment operator with the laser beam polarization; and ω is the angular frequency of the laser. It is necessary to be careful in applying the results of Ref. 5. When the value of P^2 from Ref. 5 of 19.7 a.u. is entered into Eq. (4), the result is much larger than our measured value. However, the authors of Ref. 5 originally calculated a transition moment M for absorption of one photon from each of two statistically independent laser beams:

$$M=\sum_k\left[\frac{\langle f|r|k\rangle\langle k|r'|g\rangle}{E_g-E_k-\hbar\omega'}+\frac{\langle f|r'|k\rangle\langle k|r|g\rangle}{E_g-E_k-\hbar\omega}\right] \tag{6}$$

(where the prime denotes the second laser beam). They then set $r'=r$ and $\omega'=\omega$. To avoid double counting, the resulting transition moment must be divided by 2 in order to use it in Eq. (4).[20] Since the transition moment is squared in Eq. (4), the cross section is reduced by a factor of 4. The correctly calculated cross section, $\sigma_0^{(2)}=2.8\times10^{-36}$ cm^4, is in reasonable agreement with our measurements.

B. Direct photoionization of the E,F state

Several processes fall under the general category of photoabsorption by the E,F state. In this section we con-

TABLE III. Calculated cross sections for H_2 (E,F, $v=6$)$+\hbar\omega$.

Process	σ_{355} (10^{-18} cm^2)	σ_{193} (10^{-18} cm^2)
Direct photoionization		
to $v_+=1$	0.37	0.10
to $v_+=2$	8.11	2.03
to $v_+=13$		0.52
Sum over all open channels	8.50	3.15
Photoexcitation of $^1\Sigma_u$		
autoionization	0	7.13
dissociation (neutral+ionic)	3.55	0.52

sider direct (i.e., conventional) photoionization:

$$H_2^* + \hbar\omega \rightarrow H_2^+ + e^- ,$$

which is described by the matrix element between the bound E,F state and the electronic continuum plus the bound H_2^+ state. The cross section for this process may be estimated from calculations in the literature. The work of Cohn[21] provides tabulated cross sections as a function of the ejected electron energy. We interpolated these and multiplied by the appropriate Franck-Condon factors. The results are tabulated in Table III. This approximation neglects the R dependence and the electron energy dependence of the transition moment.

More sophisticated calculations of the direct photoionization process have been carried out by Rudolph *et al.*[22] These authors reported relative cross sections for the final vibrational states, but not the absolute numbers. An estimate of the direct photoionization cross section from the E,F ($v=6$) state to $H_2^+(v=2)$ obtained from their work[20] is 1.5×10^{-18} cm^2, which is about 25% smaller than the corresponding value in Table III.

C. Photoexcitation of the $^1\Sigma_u$ autoionizing state from the E,F state

Since the measured cross section for absorption by the E,F ($v'=6$) state is larger than the calculated upper limit for direct molecular photoionization, another mechanism may play a role. Recent work in this laboratory[9,23] and elsewhere[24,25] has demonstrated that excitation to a doubly excited, dissociating autoionizing state is an important channel in the photoionization of the $C\,^1\Pi_u$ state of H_2. We therefore performed quantitative calculations to assess the role of this channel in the present situation.

The mechanism considered is illustrated in Fig. 7. The initial level is $v'=6$ of the E,F state. Excitation to the lowest $^1\Sigma_u^+$ autoionizing state is shown in the figure. This state has been calculated by Guberman[26] and its electronic configuration is $2p\sigma_u 2s\sigma_g$. It is the most likely candidate final state, because it is reached by a strong one-electron transition $2p\sigma_u \leftarrow 1s\sigma_g$ from the inner-well E $1s\sigma_g 2s\sigma_g$ component of the E,F state, and by a one-electron $2s\sigma_g \leftarrow 2p\sigma_u$ transition from the outer-well F $(2p\sigma_u)^2$ component of the E,F state. Once excitation has occurred, the nuclei start to move outward on the $^1\Sigma_u^+$ potential curve. This electronic state is unstable with respect to autoionization, which occurs as the nuclei dissociate. This process, electron emission, leads to the final state $H_2^+ + e^-$. If autoionization does not occur, the nuclei continue to follow the $^1\Sigma_u^+$ curve and ultimately reach an asymptotic state of the form $H(1s)+H^*(nl)$, or $H^+ + H^-$.

The process just described, which leads to molecular autoionization ($H_2^+ + e$), neutral dissociation ($H^* + H$), or ionic dissociation ($H^+ + H^-$), was treated using the technique developed by Hickman.[9] The method treats the dynamics of nuclear motion by solving Schrödinger's equation with a nonlocal, complex potential. Cross sections for total dissociation and molecular autoionization were obtained, as well as the distribution of final vibra-

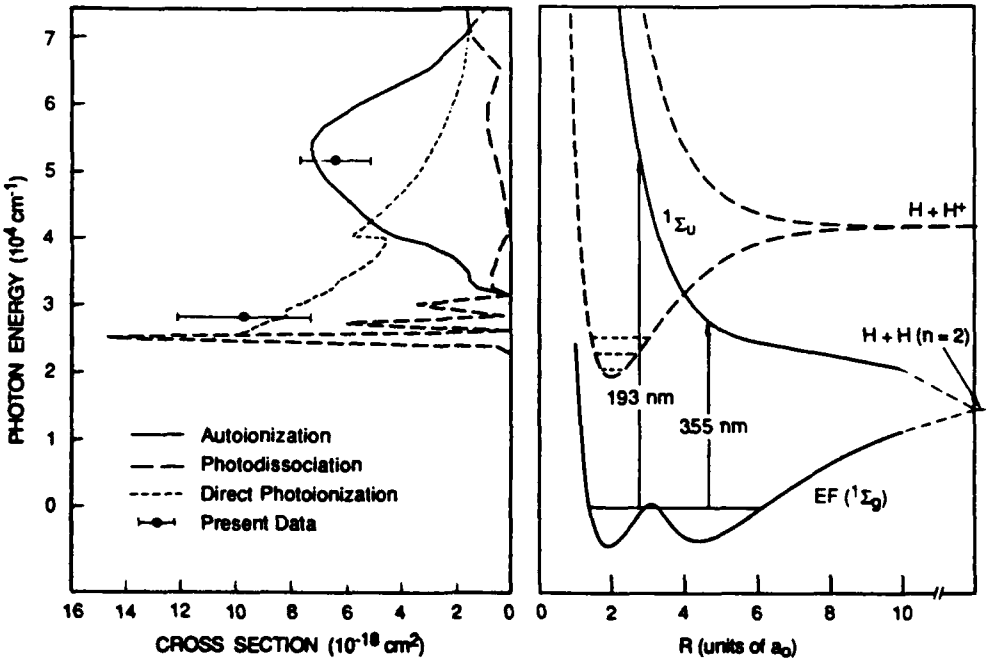

FIG. 7. (a) Calculations for direct photoionization (- - - - -), photodissociation through the $^1\Sigma_u$ state (— — —), and autoionization (——) through the $^1\Sigma_u$ state of H_2. (b) Potential curves of H_2 illustrating the mechanisms contributing to the calculations in the left panel. Notice that the energy (vertical) scales are the same in both panels, thereby clearly exhibiting the threshold behavior of all the cross sections.

tional states resulting from molecular autoionization. The necessary quantities for the calculation are the following: (1) the transition matrix element $\mu(R)$ connecting the initial E,F state with the $^1\Sigma_u^+$ state (R is the internuclear distance); (2) the potential curve for the $^1\Sigma_u^+$ state; and (3) the matrix element $V_{el}(R)$ connecting the $^1\Sigma_u^+$ state with the final-state continuum $H_2^+ + e^-$. The determination of these potentials and matrix elements is described in the following paragraph.

To calculate the transition moment $\mu(R)$ connecting the $^1\Sigma_u^+$ autoionizing state, one must take into account the R dependence of the E,F electronic wave function. This can be done in an approximate way by considering the two dominant electronic configurations, $1s\sigma_g 2s\sigma_g$ and $(2p\sigma_u)^2$. Each of these configurations corresponds to a diabatic potential curve; the avoided crossing of these curves leads to the well-known double-well nature of the E,F state. We can approximate the adiabatic electronic wave function as follows:

$$\Psi_{E,F}(R)=[\cos\Theta(R)](1s\sigma_g 2s\sigma_g)+[\sin\Theta(R)](2p\sigma_u)^2 . \tag{7}$$

Estimates of the mixing angle Θ may be obtained from the diabatic potential curves and coupling matrix elements determined by Hazi *et al.*[27] and Ross and Jungen.[28] One sets up a two-state Hamiltonian in the standard way: $H_{11}(R)$ is the energy of the $(2p\sigma_u)^2$ state; H_{22} is the energy of the $1s\sigma_g 2s\sigma_g$ state; and

$$H_{12}=v_0/[2-\delta_s(R)]^{3/2} ,$$

where $v_0=0.048$ a.u.,[27] and $\delta_s(R)$ is the quantum defect function. There is some uncertainty in the estimate of H_{12} because it was necessary to extrapolate v_0 beyond the range in which it was calculated by Hazi *et al.* The result is

$$\tan[2\Theta(R)]=2H_{12}/(H_{11}-H_{22}) .$$

We must now evaluate

$$\begin{aligned}\mu(R)&=\langle\Psi_{E,F}(R)|\mu_z|2p\sigma_u 2s\sigma_g\rangle \\ &\cong[\cos\Theta(R)]\langle 1s\sigma_g|r\cos\theta|2p\sigma_u\rangle \\ &\quad+[\sin\Theta(R)]\langle 2p\sigma_u|r\cos\theta|2s\sigma_g\rangle ,\end{aligned} \tag{8}$$

where r and θ are spherical electronic coordinates.

The first matrix element is for the $2p\sigma_u \leftarrow 1s\sigma_g$ core transition and has been evaluated by Bates.[29] Its value is $-R/2$ times a correction factor close to unity. The second matrix element is for the $2s\sigma_g \leftarrow 2p\sigma_u$ transition. It was evaluated numerically using single center wave functions determined from quantum defects. The results are well approximated by the polynomial $1.571-0.3807R+0.06268R^2$ (atomic units are used).

The $^1\Sigma_u^+$ potential curve has been calculated by Guberman.[26] The matrix element $V_{el}(R)$ is obtained from the resonance width $\Gamma(R)$ calculated by Tennyson and Noble,[30] using the relation

$$V_{el}(R)=[\Gamma(R)/2\pi]^{1/2} .$$

Tennyson and Noble calculated $\Gamma(R)$ for $R\leq 2.8$ a.u.; for larger values we took the value at $R=2.8$ a.u.

With these potential curves, and the estimates of the matrix elements, we can treat photoexcitation of the $^1\Sigma_u$ autoionizing state. The calculated results are presented and compared with our experimental measurements in Sec. IV.

IV. DISCUSSION

The measurements of the two-photon excitation ($E,F \leftarrow X$) cross section are in reasonable agreement with theory, as discussed in Sec. III A. The excitation process is straightforward and appears to need no further discussion.

Photoabsorption by the E,F ($v'=6$) state is more complex, because several alternate channels are available. We write several possibilities schematically as follows:

$$H_2^*(E,F)+\hbar\omega\rightarrow\begin{cases} H_2^+ + e^- , & \text{(9a)} \\ H_2^{**}\rightarrow H_2^+ + e^- , & \text{(9b)} \\ H_2^{**}\rightarrow H^* + H , & \text{(9b')} \\ H_2^{**}\rightarrow H^+ + H^- , & \text{(9b'')} \\ H + H^+ + e^- . & \text{(9c)}\end{cases}$$

Some of these channels have already been observed or discussed in the literature. Direct photoionization, (9a), is well known.[22] Channels (9b), (9b'), and (9b'') denote the excitation and subsequent decay of highly excited autoionizing states. Competition between autoionization and dissociation of these channels has been studied.[31] Channel (9c) is possible for sufficiently energetic photons, and has been inferred from observations of proton production.[10] A complicating feature of the experimental analysis of this channel is that other possible sources of H^+ ions are photoionization of the excited atomic hydrogen, H^*, produced by (9b'), or photodissociation of H_2^+.

Previous experiments have provided relative cross sections for several of the channels listed in (9). For example, the photoelectron energy distribution has been measured for (9) at 193 nm and provides evidence of a strongly non-Franck-Condon distribution of final vibrational states of H_2^+.[32,33] These results suggest that (9a) is not the only important channel. The present work provides complementary information, because absolute cross sections are measured and compared with theoretical calculations. Since the measured cross section for photoabsorption was significantly larger than the theoretically calculated cross section for channel (9a), additional channels probably play a role.

Theoretical calculations were carried out for comparison with the experimental data, which were obtained at values of $\hbar\omega$ corresponding to 355 and 193 nm. The calculations treat channels (9a), (9b), (9b'), and (9b''), for which estimates of the coupling terms could be obtained as described in Sec. III. These calculations suffice to demonstrate the importance of channels (9b), (9b'), and (9b''). Coupling terms to treat channel (9c) have not been

TABLE IV. Comparison of experimental and theoretical cross sections.

	$\sigma_0^2(E,F\ (v'=6)\leftarrow(v''=0))$ $(10^{-36}\ \text{cm}^4)$	$\sigma_{abs}(E,F\ (v''=6)+193\ \text{nm})$ $(10^{-18}\ \text{cm}^2)$	$\sigma_{abs}(E,F\ (v''=6)+355\ \text{nm})$ $(10^{-18}\ \text{cm}^2)$
Experimental	2.0±0.9	6.4±1.3	9.7±2.4
Calculated	2.8	10.8	12

calculated, and thus only qualitative comments can be made about this channel.

The theoretical calculations are summarized in Table III and in Fig. 7. An interesting implication of the calculations is that the relative importance of the various channels (9) changes dramatically with photon energy. This behavior can be best understood by examining Fig. 7. Cross sections for the various channels are shown. The short-dashed curve is direct photoionization, and is summed over all open final vibrational channels. It is shown for energies above the threshold for excitation of the $v=2$ vibrational state of H_2^+. The jump at about 40000 cm^{-1} corresponds to the opening of the $v=13$ state of the ion. The Franck-Condon factor for this state (0.089) is second only to that for the $v=2$ state (0.754), and comes from the portion of the wave function in the outer F well. The long-dashed curve is photodissociation (including both neutral and ionic channels) on the $^1\Sigma_u$ autoionizing state. The details of this curve are uncertain because of the approximate transition matrix element used, but the general features make physical sense. The threshold occurs at the energy at which $H(n=2)+H$ may be formed. The oscillatory structure reflects the oscillations of the vibrational wave function in the outer well. In the region of oscillations, photodissociation is effectively the only available channel. The overlap between the dissociating wave function (H^*+H) and the H_2^+ vibrational wave functions is negligible up to about 30000 cm^{-1}. Above this energy, the solid curve starts to rise. This curve corresponds to photoexcitation of the $^1\Sigma_u$ state, followed by autoionization, which can only be large when the wave function of the dissociating state (determined by the photon energy) has a good overlap with the wave functions of the open vibrational channels. It is interesting to note that the oscillations in the photodissociation curve are quenched once autoionization becomes probable.

These calculations suggest the following interpretation of the observed photoabsorption signal. At 355 nm, the process is predominantly direct photoionization, with a small component of photodissociation. Dissociative ionization, (9c), and ionic dissociation, (9b''), are not energetically allowed. At 193 nm, direct photoionization is much smaller, and photoexcitation of the $^1\Sigma_u$ state followed by autoionization is quite important. Dissociative ionization is possible at this energy, but our present data do not distinguish between the production of H_2^+ and H^+ ions. Anderson *et al.*[32] argued that less than 5% of all the ions were H^+, although Buck *et al.*[10] measured this fraction to be about 33%. Further studies are in progress to investigate this point.

We find that the sum of the calculated cross sections for (9a), (9b), (9b'), and (9b'') compares reasonably well with the measured data, as summarized in Table IV. Channels (9a) and (9b) may interfere, so that the total cross section may not be equal to the sum of the cross sections calculated for individual channels. We have not taken that into account. The crucial point we wish to make is that the measured cross section for photoabsorption is larger than the cross section calculated for direct photoionization (a factor of 2 larger at 193 nm). The additional channels considered clearly provide a substantial contribution to the total signal.

V. CONCLUSIONS

The measured integrated two-photon excitation cross section, $\sigma_0^{(2)}=(2.0\pm0.9)\times10^{-36}\ \text{cm}^4$, was in good agreement with the calculated value, $\sigma_0^{(2)}=2.8\times10^{-36}\ \text{cm}^{-4}$, for the H_2 $E,F\ ^1\Sigma_g^+$ $(v'=6)\leftarrow X\ ^1\Sigma_g^+$ $(v''=0)$ $Q(1)$ transition. The cross section for absorption by the excited E,F state of a third 193-nm photon, $\sigma_{abs}=(6.4\pm1.3)\times10^{-18}$ cm^2, was found to be substantially larger than our estimated value for direct photoionization, $3.2\times10^{-18}\ \text{cm}^2$. Excitation of the $^1\Sigma_u$ dissociating, autoionizing state was treated and shown to contribute significantly to the photoabsorption. Agreement was good between theory and experiment for absorption by the E,F state of a 355-nm photon. The sum of cross sections calculated for the separate channels was $12\times10^{-18}\ \text{cm}^2$; we measured $\sigma_{abs}=(9.7\pm2.4)\times10^{-18}\ \text{cm}^2$.

The technique of two-photon excited fluorescence (TPEF) appears promising as an analytical technique to measure densities of vibrationally excited H_2. Scaling from our demonstrated signal-to-noise ratios for $v''=0$, we estimate that densities of $10^{10}\ \text{cm}^{-3}$ per quantum state could be detected by using TPEF, using a laser pulse of 10 mJ focused to $10^{-2}\ \text{cm}^{-2}$ with a 10-ns pulse length. If the two-photon absorption cross sections for $v''=1$–14 are as large as the cross section reported here for $v''=0$, it should be possible to determine the vibrational state distributions in the multicusp H^- ion sources currently under development.[6,34]

Note added. The theoretical value of $\sigma_0^{(2)}$ has recently been reevaluated by Huo.[36] The new value is 3.6×10^{-36} cm^4. This will be discussed further in subsequent publications.

ACKNOWLEDGMENTS

This work was sponsored by the U.S. Air Force Office of Scientific Research, under Contract Nos. F49620-88-C-0112 and F49620-88-K-0005. Helpful conversations are acknowledged with Dr. Winifred Huo concerning the work of Ref. 22.

*Present address: Optical Shields, Ltd., 1390 Willow Rd., Menlo Park, CA 94025.
†Present address: Deacon Research, 900 Welch Rd., Ste. 203, Palo Alto, CA 94304.

[1]H. Eichert and M. Fischer, Int. J. Hydrogen Energy **11**, 117 (1986).
[2]W. T. Huntress, Jr., Adv. At. Mol. Phys. **10**, 295 (1974).
[3]H. Pummer, H. Egger, T. S. Luk, T. Srinivasan, and C. K. Rhodes, Phys. Rev. A **28**, 795 (1983).
[4]E. W. Rothe, G. S. Ondrey, and P. Andresen, Opt. Commun. **58**, 113 (1986).
[5]W. M. Huo and R. L. Jaffe, Chem. Phys. Lett. **101**, 463 (1983).
[6]R. L. York, R. R. Stevens, K. N. Leung, and K. W. Ehlers, Rev. Sci. Instrum. **55**, 681 (1984).
[7]D. C. Robie, L. E. Jusinski, and W. K. Bischel (unpublished).
[8]C. Cornaggia, A. Giusti-Suzor, and Ch. Jungen, J. Chem. Phys. **87**, 3934 (1987).
[9]A. P. Hickman, Phys. Rev. Lett. **59**, 1553 (1987).
[10]J. D. Buck, D. H. Parker, and D. W. Chandler, J. Phys. Chem. **92**, 3701 (1988).
[11]W. K. Bischel, D. J. Bamford, and L. E. Jusinski, Appl. Opt. **25**, 1215 (1986).
[12]D. J. Bamford, L. E. Jusinski, and W. K. Bischel, Phys. Rev. A **34**, 185 (1986).
[13]J. D. Buck, S. Kroll, and W. K. Bischel (unpublished); T. Ebata, N. Mikami, and M. Ito, J. Chem. Phys. **78**, 1132 (1983).
[14]D. C. Robie, J. D. Buck, and W. K. Bischel (unpublished).
[15]D. J. Kligler and C. K. Rhodes, Phys. Rev. Lett. **40**, 309 (1978).
[16]R. P. Saxon and J. Eichler, Phys. Rev. A **34**, 199 (1986).
[17]M. Glass-Maujean, P. Quadrelli, and K. Dressler, At. Data Nucl. Data Tables **30**, 274 (1984).
[18]G. Herzberg, *Molecular Spectra and Molecular Structure I. Spectra of Diatomic Molecules*, 2nd ed. (Van Nostrand, New York, 1950).
[19]D. J. Bamford, A. P. Hickman, M. J. Dyer, and W. K. Bischel, J. Opt. Soc. Am. B **5**, 1369 (1988).
[20]W. M. Huo (personal communication).
[21]A. Cohn, J. Chem. Phys. **57**, 2456 (1972).
[22]H. Rudolph, D. L. Lynch, S. N. Dixit, V. McKoy, and W. M. Huo, J. Chem. Phys. **86**, 1748 (1987).
[23]E. Y. Xu, T. Tsuboi, R. Kachru, and H. Helm, Phys. Rev. A **36**, 5645 (1987).
[24]W. A. Chupka, J. Chem. Phys. **87**, 1488 (1987).
[25]M. A. O'Halloran, S. T. Pratt, P. M. Dehmer, and J. L. Dehmer, J. Chem. Phys. **87**, 3288 (1987).
[26]S. L. Guberman, J. Chem. Phys. **78**, 1404 (1983).
[27]A. U. Hazi, C. Derkits, and J. N. Bardsley, Phys. Rev. A **27**, 1751 (1983).
[28]S. Ross and Ch. Jungen, Phys. Rev. Lett. **59**, 1297 (1987).
[29]D. R. Bates, J. Chem. Phys. **19**, 1122 (1951).
[30]J. Tennyson and C. J. Noble, J. Phys. B **18**, 155 (1985).
[31]J. W. J. Verschuur, L. D. Noordam, J. H. M. Bonnie, and H. B. van Linden van den Heuvell, Chem. Phys. Lett. **146**, 283 (1988).
[32]S. L. Anderson, G. D. Kubiak, and R. N. Zare, Chem. Phys. Lett. **105**, 22 (1984).
[33]E. Y. Xu, A. P. Hickman, R. Kachru, and H. Helm (unpublished).
[34]K. N. Leung, G. J. DeVries, K. W. Ehlers, L. T. Jackson, J. W. Stearns, M. D. Williams, M. G. McHarg, D. P. Ball, W. T. Lewis, and P. W. Allison, Rev. Sci. Instrum. **58**, 235 (1987).
[35]K. P. Huber and G. Herzberg, *Molecular Spectra and Molecular Structure IV. Constants of Diatomic Molecules* (Van Nostrand, New York, 1979).
[36]W. M. Huo (personal communication).

Appendix B

BANDWIDTH AND TUNING RANGE OF AN ArF LASER MEASURED BY 1 + 1 RESONANTLY ENHANCED MULTIPHOTON IONIZATION OF NO

(Accepted for publication in Applied Optics)

BANDWIDTH AND TUNING RANGE OF AN ArF LASER MEASURED BY 1 + 1 RESONANTLY ENHANCED MULTIPHOTON IONIZATION OF NO

Daniel C. Robie, Jesse D. Buck, and William K. Bischel
SRI International
Molecular Physics Laboratory
Menlo Park, CA 94025

ABSTRACT

The tuning range and bandwidth of an ArF laser were measured using 1 + 1 resonantly enhanced multiphoton ionization of NO. Operated as an injection-seeded oscillator/amplifier combination, the tuning range was 51560 to 51810 cm^{-1}; operated with single-pass amplification of the oscillator, the tuning range was 51560 to 51765 cm^{-1}. In both cases the laser bandwidth, determined from the linewidth, was $0.21 \pm .06$ cm^{-1}. Rotational lines in the $\beta(7,0)$, $\gamma(3,0)$, and $\varepsilon(0,1)$ bands were observed, including several previously unreported lines.

KEY WORDS: excimer laser, NO, multiphoton ionization, laser diagnostics.

MP 89-164
November 2, 1989

INTRODUCTION

Within the last few years, powerful tunable excimer lasers have been introduced into the laboratory. Simple techniques for the determination of the bandwidth and wavelength of these lasers in the vacuum ultraviolet are needed, particularly at the ArF (193 nm) and KrF (248 nm) laser wavelengths. Although there are several two-photon resonances, for example in H_2[1,2] and Kr[3], that could be used to calibrate the wavelength at 193 nm and 248 nm, it would be useful for a number of applications to have a calibration technique using many one-photon resonances across the ArF tuning curve, similar to the I_2 reference in the visible.[4] We report here the development of a diagnostic technique at 193 nm based on 1 + 1 resonantly enhanced multiphoton ionization (REMPI) in NO.

The beam of an ArF excimer laser is used to produce NO^+ ions through a 1 + 1 REMPI process. High-J lines of the $B^2\Pi(v' = 7) \leftarrow X^2\Pi(v'' = 0)$ (also known as the $\beta(7,0)$), the $A^2\Sigma(v' = 3) \leftarrow X^2\Pi(v'' = 0)$ (also known as the $\gamma(3,0)$), and the $D^2\Sigma(v' = 0) \leftarrow X^2\Pi(v'' = 1)$ (also known as the $\varepsilon(0,1)$) bands of NO lie within the tuning range of the ArF laser. In all of these bands we have observed rotationally resolved lines by REMPI that have not been previously reported. From the energies and widths of these lines, we have been able to measure the tuning range and bandwidth of the laser.

EXPERIMENTAL

Spectra were collected using two laser systems. Spectra over a wide tuning range were taken using a dye laser. The output of a Nd:YAG laser (Quanta-Ray DCR-2) was doubled and used to pump a tunable dye laser (Quanta-Ray PDL-2) using Rhodamine 6G dye. The visible output of the dye laser was doubled in an angle-tuned KDP crystal (Inrad Autotracker II), and the resulting UV light was focused along with the residual visible light into a Raman cell containing 80 psi of H_2 using a 50-cm lens. Light of different Stokes and anti-Stokes orders leaving the Raman cell was separated using a Pellin-Broca prism. Pulse energies of 30-80 μJ were obtained in the fourth anti-Stokes order from 190.1 to 194.8 nm. The beam was collimated, then focused with a 100-cm lens into a cell containing NO at about 0.1 torr, and ionization spectra were recorded as the laser wavelength was scanned. Assuming a twice-diffraction-limited beam, a beam diameter of 1 cm implies that the spot size at the focus was 5×10^{-6} cm^{-2}, in which case the maximum intensity at the focus was 3×10^9 W cm^{-2}.

Spectra over a narrower tuning range were taken using a Lambda-Physik EMG150MSC laser. The apparatus is diagrammed in Figure 1. ArF was the lasing medium. The laser had two discharge cavities. One end of the oscillator cavity had a 3 mm aperture, a set of prism beam expanders, and a diffraction grating (600 lines/mm, blaze angle 54°06'). The tilt of the grating was controlled by a micrometer turned with a motor controlled by an optical encoder.

The excimer laser was operated with two arrangements. In the first, the oscillator beam ran through the amplifier cavity with no optics. The beam was in that case amplified by the ArF discharge. This was called the "amplified oscillator" mode. The resulting pulse energy was 1-2 mJ. In the second arrangement, the oscillator beam was used to injection-seed the amplifier discharge, which lased on its own with unstable resonator optics. This was the "locked amplifier" mode. The resulting pulse energy was 100-120 mJ. The measured bandwidth of the beam was the same in both cases. The advantages of the locked amplifier mode are increased energy and low divergence (specified to be 0.3 mrad). The disadvantage of the locked amplifier mode is that the locking efficiency is unknown. When the amplifier is completely locked, all the photons in the pulse are within the narrow bandwidth of the laser. At locking efficiencies less than 100% (e.g., at the edges of the tuning range), some of the photons are outside of the narrow bandwidth. The total energy of the pulse does not drop proportionally. Even when the amplifier is completely unlocked the pulse energy is high. Furthermore, the broadband unlocked beam covers all the transitions in the spectrum observed. This produces background ionization that increases as the locking efficiency drops. As a result, in the locked amplifier mode we were unable to determine the effective number of laser photons at each frequency, and so were unable to normalize the ion signal for laser energy. (If the dependence of the background ion signal on the broadband power, and that of an on-resonance ion signal on the power in a narrow band, is known, then the ratio of the background ions to the ions generated on a resonance can be used to determine

the locking efficiency. For instance, if the background is proportional to the total broadband beam energy and one step of 1 + 1 REMPI on the resonance is saturated, the locking efficiency is proportional to the ratio of on-resonance ion signal to off-resonance ion signal.) The amplified oscillator mode has the advantage that nearly all the photons in the beam are within the narrow bandwidth of the laser at all frequencies within the tuning range, with the disadvantages of lower power and greater divergence.

The laser beam, with a wavelength around 193 nm, was propagated through the air. An iris located just before the cell was used to fix the beam diameter between 0.5 and 2 mm. The beam passed through a fused silica window at Brewster's angle into the cell, between two electrodes, and out another Brewster's angle window. The beam was terminated in a Laser Precision Rj7200 joulemeter. The power in the cell was determined for the collimated beams from measurements of the pulse energy at the cell exit and independent measurements of the transmittance of the cell windows and atmosphere, the pulse duration, and the beam diameter. Pulse energies at the cell center were typically 100 μJ at the center of the tuning range for the amplified oscillator mode, and 500 μJ for the locked amplifier mode. In the locked amplifier mode, the beam was collimated, with the beam area in the cell 0.02 cm^2. The pulse width was ~10 ns, so that the beam intensity was 3×10^6 W cm^{-2}. The intensity in the amplified oscillator mode was $\leq 5 \times 10^5$ W cm^{-2}.

NO (99.0% from Liquid Carbonic) flowed through the cell slowly at a pressure of 70 mtorr. (For the spectrum with the amplified oscillator, 90 mtorr of

Ar was added.) Pressure was monitored with a 10 torr capacitance manometer. Subsequent to the cell, the gas passed into a rotary oil pump.

Ions were collected on two parallel aluminum bar electrodes $6 \times 6 \times 25$ mm separated by 2 cm. These were set in a plane containing the laser beam, and connected to an Ortec 113 preamplifier in the locked amplifier mode, and to an Ortec 142PC charge-sensitive preamplifier in the amplified oscillator mode. One electrode was grounded. Bias voltage of 90 V was supplied by a battery-powered voltage divider. (Much larger signals were obtained by using 1-10 torr of 5% NO/Ar and increasing the bias voltage until dc breakdown occurred at ~300 V/cm, then dropping the voltage by 10 or 20 V. The width of the lines did not appreciably increase. Presumably the electrons were multiplied in an avalanche discharge.) The output from the preamplifier was put into a Stanford Research SR250 boxcar integrator. The output of the joulemeter was put into another boxcar channel. The boxcar integrator outputs fed an oscilloscope and a Hewlett-Packard 7090A ADC and digitizing plotter. The data was shipped to a DEC VAX for further analysis. This system was sufficiently well calibrated that absolute numbers of ions collected could be determined to one significant figure.

RESULTS

The spectra obtained are shown in Fig. 2-4. Fig. 2 was obtained with the Raman-shifted Nd:YAG-pumped dye laser. Lines from the $\gamma(3,0)$, $\beta(7,0)$, $\beta(6,0)$, and $\delta(0,0)$ ($C^2\Pi$ (v' = 0) - $X^2\Pi$ (v" = 0)), bands are clearly evident. The width of the lines is 1.3 cm^{-1}. A spectrum was run under similar conditions with

H_2 added to the cell. In addition to the NO lines, the well-known EF-X (6,0) 2 + 1 REMPI lines of H_2[1] appeared. The locations of these lines have been carefully measured, and their previously published energies[5,6] were used to determine the energies of a few NO lines nearby. The measured line energies were compared with the energies predicted using the spectroscopic constants of Huber and Herzberg.[7] The measured energies were found to be greater than the calculated energies by $+0.3 \pm 0.4$ cm^{-1}. This difference may be due to an ac Stark shift of the energy levels for the H_2 lines used for the calibration. The shift of the EF($v = 6$) levels has been predicted by Srinivasan et al. to be +1.8 MHz/MW cm^{-2} at 193 nm,[8] which would imply a shift of +0.2 cm^{-1} in the upper state of the transition. (The shift in the X state is considerably smaller.)

The power and ion spectrum from the EMG150MSC in the amplified oscillator mode is shown in Fig. 4. This spectrum was run at a scan speed of 0.09 cm^{-1}/s. The tuning range–defined as the difference between the energies of the most and least energetic identified lines–is 205 cm^{-1}, from 51560 to 51765 cm^{-1}. Dips in the baseline are due to O_2 absorption lines from the Schumann-Runge (4,0) and (7,1) bands.[9] Lines from the β(7,0) and γ(3,0) bands of NO are apparent. A complete list of the line identifications and measured vacuum wavenumbers ($\pm$ 0.5 cm^{-1}) is given in Table I. Several of these lines have not, to our knowledge, been previously observed. As demonstrated in the next section, the excitation step was saturated for the β(7,0) and ε(0,1) bands, but the ionization step was not. This implies that the number of ions detected was proportional to the pulse energy. The peak output voltage of the preamplifier

equals the charge collected on the electrodes multiplied by a manufacturer-specified gain (1.25×10^{12} V/C). We have calculated the number of ions detected per joule of pulse energy from the ratio of ion channel voltage s_{ion} to pulse energy channel voltage s_E:

$$\frac{N}{E} = \frac{1}{(1.25 \times 10^{12})geK} \frac{s_{ion}}{s_E} \qquad (1)$$

where E is the pulse energy, g is the gain of the ion channel boxcar integrator, and K is a measured proportionality constant for the pulse energy channel.

The power and ion spectrum from the EMG150MSC in the locked amplifier mode is shown in Fig. 5. It covers 250 cm^{-1}, from 51560 to 51810 cm^{-1}. It is not known whether the difference at the blue end of the range between the amplified oscillator and locked amplifier spectra is due to the laser oscillator losing its alignment, or would persist even under ideal conditions. Because of irregularities in the linearity of the spectrum, the wavenumber calibration for this spectrum was not as precise as that for the amplified oscillator spectrum. Consequently, the line positions could only be determined to within $\pm$ 1 cm^{-1}. Where these lines are not duplicates of lines found in the amplified oscillator spectrum, they are listed in Table I. In this case, the peak output voltage of the preamplifier equals the charge at its input divided by the input capacitance C (previously measured to be 83 pF). Then the voltage output of the boxcar integrator, s_{ion}, is related to the number of ions detected by Eq. (2):

$$N = \frac{S_{ion}\, C}{ge} \tag{2}$$

where g is the gain of the boxcar integrator, and e is the charge of an electron.

Fig. 6 shows a small piece of the EMG150MSC amplified oscillator spectrum including the $\gamma(3,0)\ ^{S}R_{21}$ 33.5 line. A Gaussian fit yields a FWHM for single isolated lines of $0.24 \pm 0.05\ cm^{-1}$ (7.2 ± 1.5 GHz). The bandwidth of the laser was found to be quite sensitive to the precise alignment of the grating. Over the course of recording a spectrum, the bandwidth sometimes increased. The bandwidth could always be reduced to the minimum value by readjustment of the grating.

DISCUSSION

Many factors besides laser bandwidth can affect measured linewidth. We will evaluate the contributions of various mechanisms to show how the laser bandwidth can be obtained from the measured linewidth $\Delta\nu$. As an example, we use the $P_{22}(28.5)$ line of the $\beta(7,0)$ band in the locked amplifier mode. The oscillator strength of branches of the $\beta(7,0)$ band originating at $^{2}\Pi_{3/2}$ levels has been calculated[10] as 1.3×10^{-4}. The frequency-integrated cross section for excitation in the $P_{22}28.5$ line can be evaluated from the band oscillator strength:

$$\sigma(J',J'') = \frac{\pi e^2}{m_e c} f(v',v'') \frac{S(J',J'')}{2J''+1} \tag{3}$$

$$= 1.7 \times 10^{-6}\ cm^2\ Hz.$$

S(J',J") is the Hönl-London factor[11] (S(27.5,28.5) = 27.9). The rate of absorption at the peak of the line is the product of the cross section σ_ν at the peak and the photon flux Φ. For an inhomogeneously broadened line,

$$\sigma_\nu(J',J") = 2\sqrt{\frac{\ln 2}{\pi}}\frac{1}{\Delta\nu}\sigma(J',J") \qquad (4)$$

when $\Delta\nu$ is the measured FWHM linewidth in Hz. As shown above, $\Delta\nu$ = 7.2 GHz, so for the $P_{22}(28.5)$ line

$$\sigma_\nu(27.5,28.5) = 2.2 \times 10^{-16}\ cm^2$$
$$\sigma_\nu\Phi = 6 \times 10^8\ s^{-1}$$

where Φ is the photon flux, $3 \times 10^{24}\ cm^{-2}\ s^{-1}$. The rate of stimulated emission from the excited state equals the rate of absorption from the ground state. In both modes, stimulated emission was the dominant sink on the excited state population followed by fluorescence,[12,13] with quenching[12,13] contributing significantly:

$$A = 3 \times 10^6\ s^{-1}$$
$$k_Q(NO) = 7 \times 10^5\ s^{-1}$$
$$\sigma_{ion}\,\Phi \leq 2 \times 10^5\ s^{-1}$$

where the ionization cross section measured by Rottke and Zacharias[14] at 355 nm was taken as an upper bound.

Homogeneous line-broadening mechanisms include pressure broadening ($\Delta\nu_p = 0.7$ MHz) and lifetime broadening ($\Delta\nu_\ell = 4$ MHz). Saturation broadening[15] may be evaluated from these quantities:

$$\Delta\nu_s = \sqrt{(\Delta\nu_p)^2 + (\Delta\nu_\ell)^2}\ \sqrt{1+S} \tag{5}$$

where S is the saturation parameter:

$$S \equiv \frac{\sigma_V \Phi}{A + k_Q(NO) + \sigma_{ion}\Phi} \tag{6}$$

$$= 150$$

Saturation broadening increases the homogenous linewidth to 50 MHz in the locked amplifier mode, considerably less than the Doppler width at room temperature, $\Delta\nu_D = 3.6$ GHz. We conclude that saturation broadening is not significant. The only remaining factor affecting the linewidth is the laser bandwidth $\Delta\nu_L$. The measured linewidth is related to the Doppler width and the laser bandwidth by

$$\Delta\nu = \sqrt{(\Delta\nu_D)^2 + (\Delta\nu_L)^2} \qquad (7)$$

For $\Delta\nu$ = 7.2 GHz, the laser bandwidth is 6.2 ± 1.8 GHz (0.21 ± 0.06 cm^{-1}).

CONCLUSION

We have observed several lines in the $\beta(7,0)$ band with $J'' \geq 24.5$, in the $\gamma(3,0)$ band with $J'' \geq 31.5$, and in the $\varepsilon(0,1)$ band with $J'' \geq 13.5$ (along with several lines we could not identify) that have not been previously reported. Their energies are in good agreement with predictions based on previously determined spectroscopic constants. The linewidths have been used to determine the bandwidth of a tunable ArF excimer laser. This technique can be used to monitor the wavelength and bandwidth of such a laser.

ACKNOWLEDGEMENT

This work was sponsored by the Air Force Office of Scientific Research, under Contract No. F49620-C-0112. We thank Dr. T. G. Slanger, Dr. D. L. Huestis, and Dr. P.C. Cosby for discussions of the spectroscopy and dynamics of NO.

REFERENCES

1. D.J. Kligler and C.K. Rhodes, "Observation of two-photon excitation of the H_2 E,F $^1\Sigma$ state", Phys. Rev. Lett. **40**, 309 (1978).

2. D.J. Kligler, J. Bokor and C.K. Rhodes, "Collisional and radiative properties of the H_2 E,F$^1\Sigma_g^+$ state", Phys. Rev. A **21**, 607 (1980).

3. W.K. Bischel, J. Bokor, D.J. Kligler and C.K. Rhodes, "Nonlinear optical processes in atoms and molecules using rare-gas halide lasers", IEEE J. Quant. Elec. **QE-15**, 380 (1979).

4. S. Gerstenkorn and P. Luc, *Atlas du spectre d'absorption de la molecule d'iode* (Editions du CNRS, Paris, 1978).

5. I. Dabrowski, "The Lyman and Werner bands of H_2", Can. J. Phys. **62**, 1639 (1984).

6. P. Senn and K. Dressler, "Spectroscopic identification of rovibronic levels lying above the potential barrier of the EF$^1\Sigma_g^+$ double-minimum state of the H_2 molecule", J. Chem. Phys. **87**, 6908 (1987).

7. K.P. Huber and G. Herzberg, *Constants of diatomic molecules* (Van Nostrand Reinhold, New York, 1979), pp. 474-480.

8. T. Srinivasan, H. Egger, H. Pummer, and C.K. Rhodes, "Generation of extreme ultraviolet radiation at 79 nm by sum frequency mixing", IEEE J. Quant. Elec. **QE-19**, 1270 (1983).

9. M. Nicolet, S. Cieslik, and R. Kennes, "Rotational structure and absorption cross sections from 300 K to 190 K of the Schumann-Runge bands", Aeronomica Acta A, no.318 (1987).

10. R. Gallusser and K. Dressler, "Multistate vibronic coupling between the excited $^2\Pi$ states of the NO molecule", J. Chem. Phys. **76**, 4311 (1982).

11. H. Okabe, *Photochemistry of small molecules* (Wiley-Interscience, New York, 1978), p. 39.

12. K. Shibuya and F. Stuhl, "Fluorescence lifetime and collisional quenching of the predissociative NO $B^2\Pi(v'=7)$ state", Chem. Phys. **79**, 367 (1983).

13. W. Hack, R.K. Sander, J.J. Valentini, and N.S. Nogar, "Dynamics of $^{14}N^{16}O$ and $^{15}N^{18}O$ excited with an ArF-exciplex laser at 193 nm", Mol. Phys. **56**, 977 (1985).

14. H. Rottke and H. Zacharias, "Photoionization of single rotational levels in excited $B^2\Pi$, $C^2\Pi$, and $D^2\Sigma^+$ states of $^{14}N^{16}O$", J. Chem. Phys. **83**, 4831 (1985).

15. W. Demtröder, *Laser spectroscopy* (Springer-Verlag, Berlin, 1982), pp. 105-111.

TABLE I. ABSORPTION LINES OBSERVED IN THE TUNING RANGE OF THE ArF LASER.

Identifications are shown when known. Lines from both the amplified oscillator and the locked amplifier spectra are included. Calculated line energies were obtained using the spectroscopic constants of Huber and Herzberg.[7]

band	line	observed $\tilde{\nu}$/cm^{-1}	calculated $\tilde{\nu}$/cm^{-1}
ε(0,1)	$R_{11}17.5$	51558.6	51561.1
ε(0,1)	$^{S}R_{21}13.5$	51570.1	51570.1
γ(3,0)	$Q_{11}45.5$	51572.3	51572.0
γ(3,0)	$^{S}R_{21}31.5$	51575.8	51575.9
		51581.1	
		51581.7	
ε(0,1)	$^{S}R_{21}14.5$	51585.5	51585.7
γ(3,0)	$R_{11}38.5$	51586.6	51586.5
ε(0,1)	$R_{11}19.5$	51591.1	51590.4
ε(0,1)	$R_{22}22.5$	51592.2	51592.5
γ(3,0)	$Q_{11}46.5$	51594.4	51593.1
		51596.8	
γ(3,0)	$^{S}R_{21}32.5$	51599.1	51597.8
ε(0,1)	$^{S}R_{21}15.5$	51602.2	51602.0
β(7,0)	$P_{11}31.5$	51605.0	51605.5
β(7,0)	$P_{22}29.5$	51606.3	51606.5
β(7,0)	$R_{11}34.5$	51607.6	51608.1
ε(0,1)	$R_{22}23.5$	51612.2	51612.2
		51616.8	
ε(0,1)	$^{S}R_{21}16.5$	51618.9	51619.0
γ(3,0)	$^{S}R_{21}33.5$	51620.1	51620.3
ε(0,1)	$R_{11}21.5$	51622.3	51622.3
		51623.6	
γ(3,0)	$R_{11}40.5$	51630.0	51630.0
ε(0,1)	$R_{22}24.5$	51630.7	51632.5
		51636.2	
ε(0,1)	$^{S}R_{21}17.5$	51636.6	51636.6
		51637.5	
ε(0,1)	$R_{11}22.5$	51639.7	51639.2
γ(3,0)	$^{S}R_{21}34.5$	51643.0	51643.5
		51647.3	
β(7,0)	$P_{22}28.5$	51648.7	51648.3
β(7,0)	$P_{11}30.5$	51649.7	51649.5
β(7,0)	$R_{11}33.5$	51651.8	51651.7

β(7,0)	$R_{22}31.5$	51652.7	51652.3
ε(0,1)	$^{S}R_{21}18.5$	51654.4	51654.9
ε(0,1)	$R_{11}23.5$	51655.6	51656.8
		51660.2	
γ(3,0)	$^{S}R_{21}35.5$	51666.8	51666.9
		51670.4	
ε(0,1)	$^{S}R_{21}19.5$	51673.5	51673.8
ε(0,1)	$R_{11}24.5$	51674.9	51675.0
		51683.5	
		51686.3	
β(7,0)	$P_{22}27.5$	51688.2	51688.4
β(7,0)	$P_{11}29.5$	51691.9	51691.7
β(7,0)	$R_{22}30.5$	51692.8	51692.4
β(7,0)	$R_{11}32.5$	51694.0	51693.9
γ(3,0)	$R_{11}43.5$	51699.2	51698.8
		51701.0	
		51704	
γ(3,0)	$^{S}R_{21}37.5$	51714.1	51715.1
γ(3,0)	$R_{11}44.5$	51722	51722.7
β(7,0)	$P_{22}26.5$	51727.0	51727.1
β(7,0)	$R_{22}29.5$	51730	51731.1
β(7,0)	$P_{11}28.5$	51732	51732.7
β(7,0)	$P_{22}25.5$	51764.6	51764.6
β(7,0)	$R_{22}28.5$	51770	51768.5
β(7,0)	$P_{11}27.5$	51773	51772.4
β(7,0)	$P_{22}24.5$	51801	51800.7
β(7,0)	$P_{11}26.5$	51810	51810.7

FIGURE CAPTIONS

Figure 1. Apparatus diagram for the locked amplifier mode. For the amplified oscillator mode, 90 mtorr of Ar was added.

Figure 2. 1 + 1 REMPI spectrum of NO using a Nd:YAG-pumped dye laser. Laser bandwidth, as determined from the linewidths, was 1.3 cm^{-1}.

Figure 3. 1 + 1 REMPI spectrum of NO using a tunable ArF laser in the amplified oscillator mode. In this mode, the ion signal can be normalized by the pulse energy; the vertical axis is ions detected per joule of pulse energy. Measured linewidth is 0.24 $\pm$ 0.05 cm^{-1} (7.2 $\pm$ 1.5 GHz). Accounting for the Doppler broadening, the laser bandwidth is 0.21 $\pm$ 0.06 cm^{-1} (6.2 $\pm$ 1.8 GHz).

Figure 4. 1 + 1 REMPI spectrum of NO using a tunable ArF laser in the locked amplifier mode. In this mode, the lack of information on locking efficiency precludes pulse energy normalization. The scale on the horizontal axis is different from that of Fig. 3. The measured linewidth, and therefore the laser bandwidth, is the same as that of Fig. 3.

Figure 5. The $^{S}R_{21}$ 33.5 line of the γ (3,0) band.

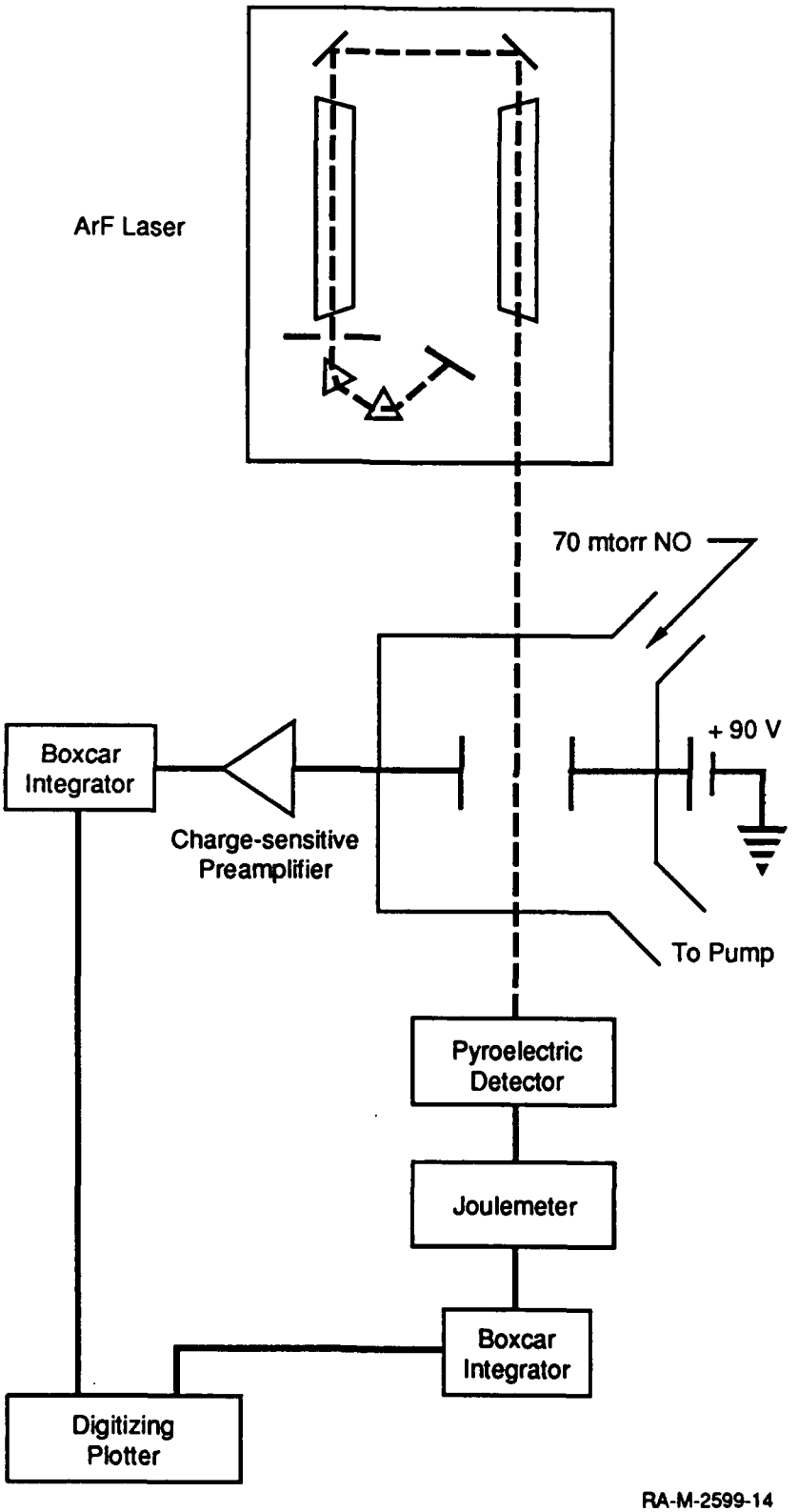
ArF Laser
70 mtorr NO
+ 90 V
Boxcar Integrator
Charge-sensitive Preamplifier
To Pump
Pyroelectric Detector
Joulemeter
Boxcar Integrator
Digitizing Plotter
RA-M-2599-14

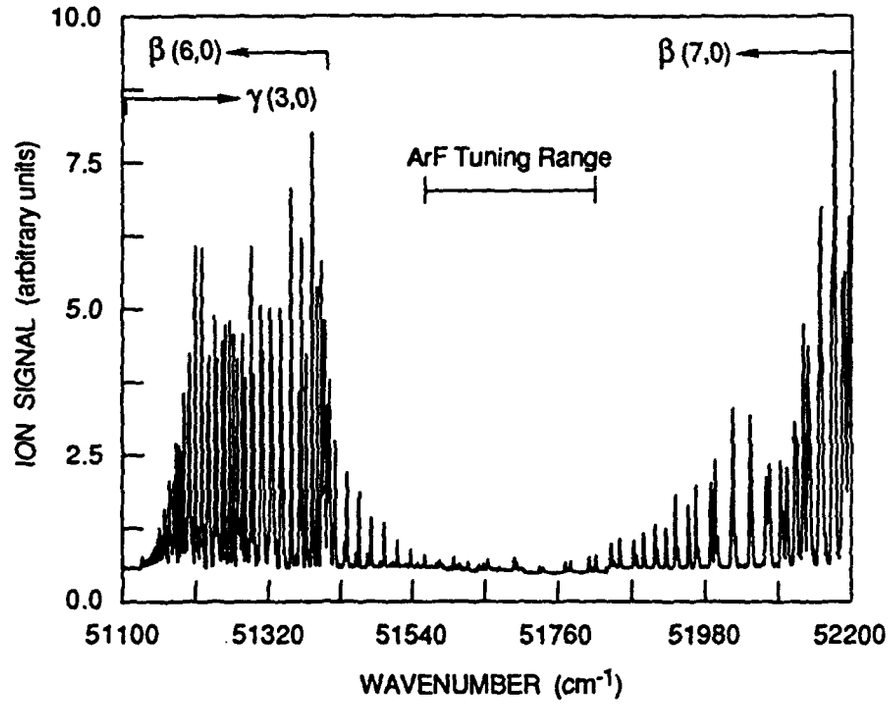
10.0
7.5
5.0
2.5
0.0
ION SIGNAL (arbitrary units)
β (6,0)
γ (3,0)
β (7,0)
ArF Tuning Range
51100
51320
51540
51760
51980
52200
WAVENUMBER (cm-1)
RA-2599-17

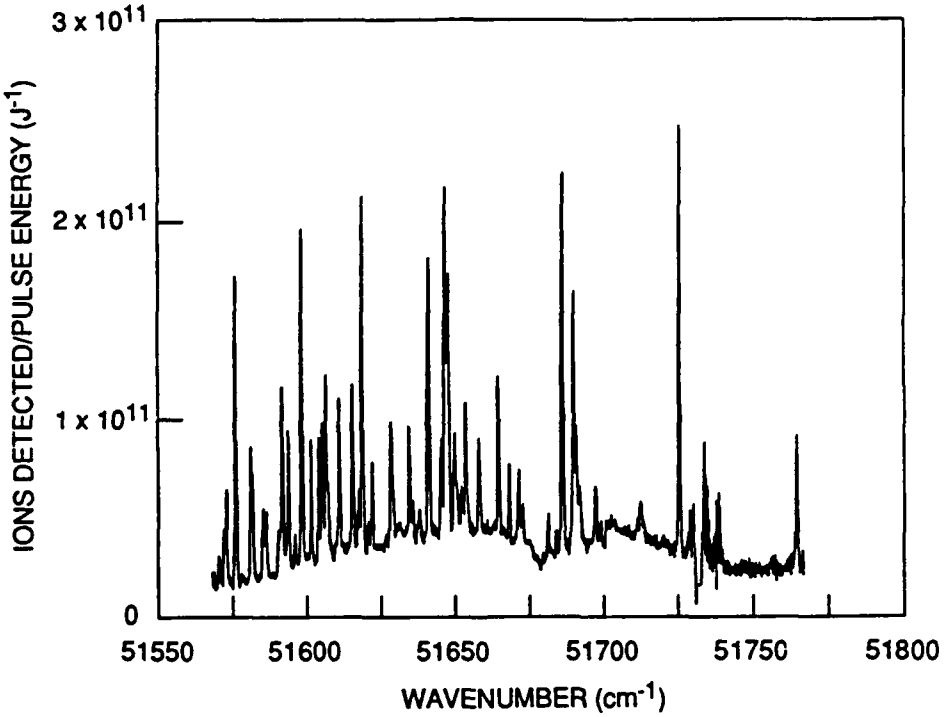
3 x 10^11
2 x 10^11
1 x 10^11
0
IONS DETECTED/PULSE ENERGY (J^-1)
51550
51600
51650
51700
51750
51800
WAVENUMBER (cm^-1)

RA-2599-16

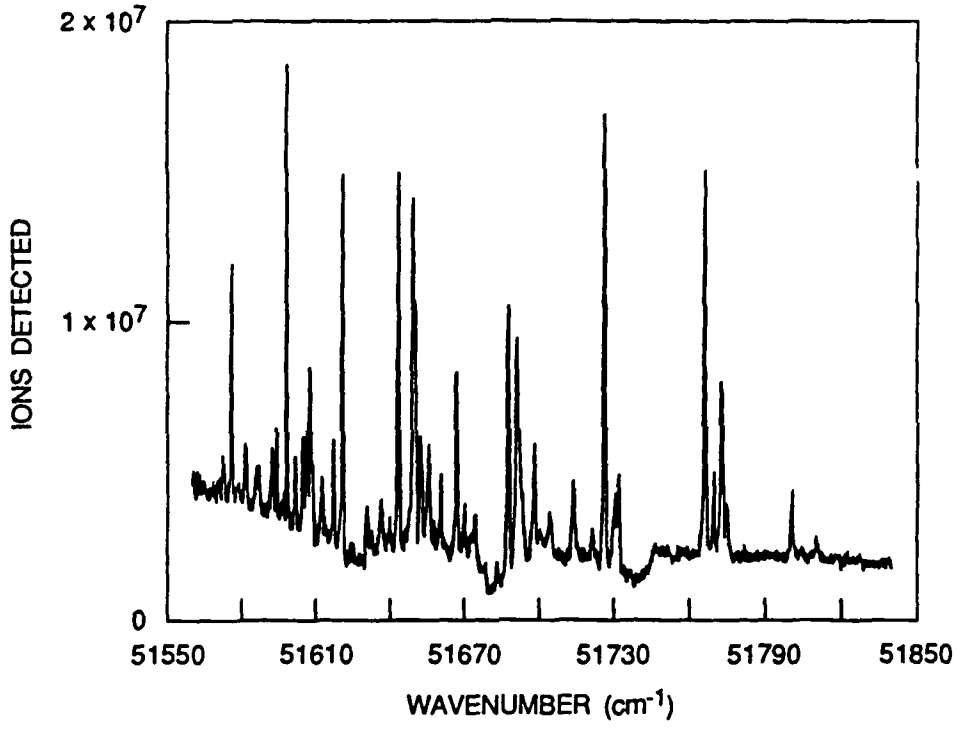
2 x 10^7
1 x 10^7
0
IONS DETECTED
51550
51610
51670
51730
51790
51850
WAVENUMBER (cm^-1)
RA-2599-15

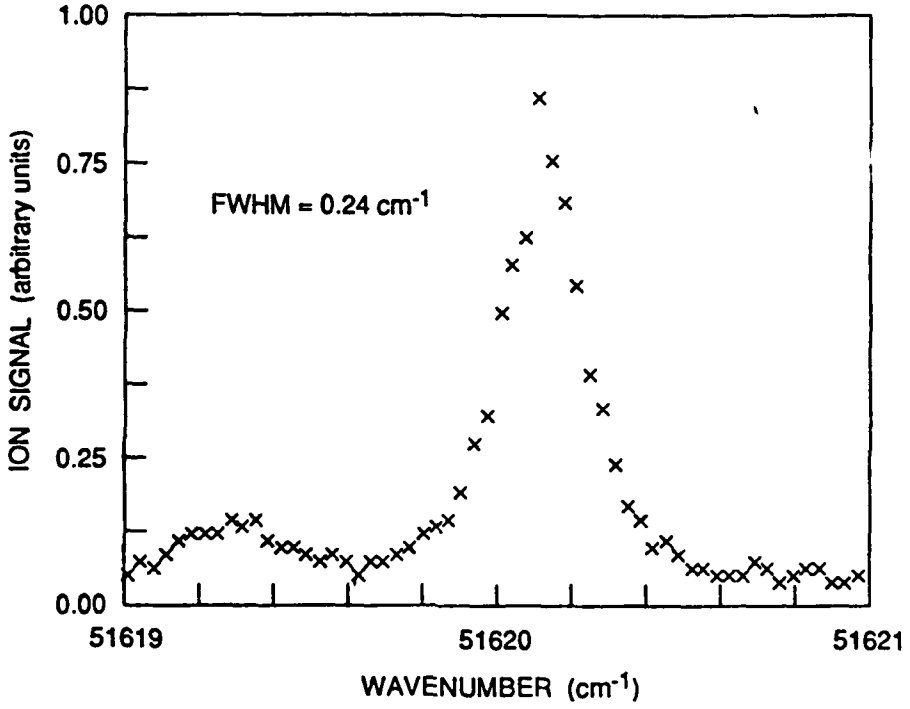
1.00
0.75
0.50
0.25
0.00
ION SIGNAL (arbitrary units)
FWHM = 0.24 cm-1
51619
51620
51621
WAVENUMBER (cm-1)

RA-2599-18

Appendix C

GENERATION OF HIGHLY VIBRATIONALLY EXCITED H_2 AND DETECTION BY 2 + 1 RESONANTLY ENHANCED MULTIPHOTON IONIZATION

(Accepted for publication in Applied Physics Letters)

GENERATION OF HIGHLY VIBRATIONALLY EXCITED H_2 AND DETECTION BY 2+1 RESONANTLY ENHANCED MULTIPHOTON IONIZATION

Daniel C. Robie,[a] Leonard E. Jusinski, and William K. Bischel[b]
SRI International, Molecular Physics Laboratory
Menlo Park, CA 94025

ABSTRACT

We report the first detection by optical means of highly vibrationally excited H_2 $X\,^1\Sigma_g^+$ ($v_x = 6$ to 11). Vibrationally excited H_2 was generated using a recently discovered hot-wire effect in H_2 gas and was detected in 40 bands with 2+1 resonantly enhanced multiphoton ionization (REMPI) via the EF state ($v_{EF} = 0$ to 14). Rotational temperatures are in the range 200-650 K, well below that required for thermal excitation of the observed vibrational levels.

---

a) Present Address: Department of Chemistry, University of Southern California, Los Angeles, CA 90089
b) Present Address: Coherent Inc., 3210 Porter Drive, Palo Alto, CA 94304

It is believed that the main source of H^- in hydrogen plasmas is dissociative attachment to vibrationally excited $H_2(X^1\Sigma_g^+)$.[1,2] To examine this, it is desirable to measure the populations of high vibrational levels of $H_2(X^1\Sigma_g^+)$ inside the plasma. While developing a technique to do this, we have constructed a source of highly vibrationally excited H_2. Using 2+1 resonantly enhanced multiphoton ionization (REMPI) via vibrational levels of the double-minimum $EF^1\Sigma_g^+$ state, we have detected $H_2(X, v_x = 0, 2, 4\text{-}11)$. This is the first report of the detection of $H_2(X, v_x \geq 6)$ by optical means, although previous detection of $H_2(2 \leq v_x \leq 5)$ has been reported by coherent anti-Stokes spectroscopy,[3] 3+1 REMPI,[4] vacuum ultraviolet absorption,[5] and 2+1 REMPI.[6,7]

The apparatus is diagrammed in Figure 1. Vibrationally excited H_2 was generated using a hot-wire effect discovered recently by Hall et al.[8] and Eenshuistra et al.[4] in which H atoms formed by dissociation on a hot wire undergo recombinative desorption on cool walls. A tantalum wire 23 cm long (initially .38 mm in diameter) was heated with 7.5 A of dc current at 20 V. The wire was enclosed in a water-cooled stainless steel cylinder 15 cm long and 2.5 cm in diameter. H_2 flowed slowly into the cylinder at the base of the wire. The pressure in the cylinder was 10 mtorr; average residence time of a molecule in the cylinder was 12 ms, during which it underwent 1×10^3 collisions with the walls. Attached to the end of the cylinder was a quartz cylinder, 1.5 cm long, with grids at both ends. The laser beam passed through the quartz cylinder via two 1/8"-diameter holes drilled in the sides. Surrounding the quartz cylinder was a diffusion-pumped chamber, where the pressure was $\sim 10^{-2}$ times that in the cylinder. Coaxial with the cylinder was an 18-cm drift tube for time-of-flight mass separation, ending with an EMI 9642 B electron multiplier. The electron multiplier cathode, the drift tube, and the two grids attached to the quartz cylinder were all connected to high voltage supplies. Potentials were adjusted to give the best mass resolution and narrowest peaks for H^+ and H_2^+ ions; typical voltages were 0 V, -100 V, -500 V, and -2500 V, from the first grid to the cathode. The ion signals

from the electron multiplier were amplified by a Pacific Instruments 2A50 video amplifier and fed into boxcar averagers, so that the H^+ and H_2^+ peaks could be followed separately.

Tunable laser light was generated by a Nd:YAG-pumped doubled dye laser, the output of which could be H_2-Raman-shifted. The desired wavelength was selected with a crystalline quartz or Homosil Pellin-Broca prism, and focused with lenses of 20 to 100 cm focal length into the center of the quartz cylinder. The H^+ and H_2^+ signals were recorded as the wavelength was varied over practically all of the spectral region between 246.8 nm and 286.3 nm, and smaller wavelength intervals around 193, 202, 210, 220, and 232 nm.

At the blue end of the scanned region, the spectrum is relatively simple, composed only of bands originating from $H_2(v_x \leq 7)$. At the red end there is substantial congestion from 3+1 REMPI bands, originating from $H_2(v_x = 0)$ and resonant with the B, B', C, and D states.[9-11] (We also detected 3+1 REMPI lines in the H Lyman progression from 285 nm to 274 nm for excitation to n = 5 to 12.) Figure 2 shows a part of the H^+ spectrum, from 264.5 to 266.6 nm, including the 5-8, 8-9, 11-10, and 13-11 bands. (Line assignments for these bands are from Dabrowski[12] and Senn and Dressler.[13]) The H^+ spectrum is richer and more intense than the H_2^+ spectrum in this wavelength region. 3+1 REMPI bands originating from $H_2(X,v_x=0)$ are also identified. (Line assignments for these bands are from Dabrowski,[12] Monfils,[14] and Namioka.[15]) In other spectra, we identified in 3+1 REMPI the 8-0 Werner (C-X) band and the 14-0, 24-0, and 25-0 Lyman (B-X) bands.

Table I shows all the bands for which the Q1 line was observed (marked with an X). Also, all the bands lying within the spectral region scanned for which the location of the Q1 line was unobscured, but for which it was not observed, are marked with an O. In addition, lines of the 7-2, 4-4, 7-7, and 11-8 bands were observed, for a total of 40 observed bands. No bands originating from the highest vibrational levels ($12 \leq v_x \leq 14$) were observed, presumably due to low populations.

The density of $H_2(v_x=9)$, and the sensitivity of the apparatus, can be estimated using known apparatus parameters. We estimate that 600 ions per pulse struck the plate of the electron multiplier at the peak of the 8-9 Q1 line. The ion collection efficiency of the apparatus has been measured at ≈0.1. From Quanta-Ray specifications we estimate the doubled dye laser beam to be twice-diffraction-limited, so that with a 35-cm lens the beam area at the focus was $\sim 5 \times 10^{-6}$ cm^2. The photon flux was then $\sim 10^{29}$ cm^{-2}s^{-1}. If the peak two-photon absorption and excited state ionization cross sections are approximately the same for this band as for the 6-0 band (10^{-47} cm^{4}s and 10^{-17} cm^2, respectively[16]), both the two-photon excitation and the excited state ionization steps were saturated. The ionization volume was approximately 5×10^{-6} cm^3, based on Gaussian beam parameters of a twice-diffraction-limited beam. These estimates imply that the density of $H_2(v_x=9, J=1)$ in the source was $\sim 10^9$ cm^{-3}. The signal-to-noise ratio of the 8-9 Q1 line was 100:1, so the minimum density detectable was $\sim 10^7$ cm^{-3}. The ratio of the density of $H_2(v_x=9)$ to the density of gas in the cell was 3×10^{-6}. This is consistent with the observations of Hall et al.,[8] who estimated the same ratio in their system to be 10^{-6}.

In earlier work, Hall et al. estimated the rotational temperature to be near room temperature.[8] To determine rotational temperatures from our data, it is necessary to know the wavelength and rotational state dependence of the two-photon excitation cross section, the excited state absorption cross section, and the branching ratio for H^+ production after absorption. Recent calculations[17] and previous measurements of J-dependence in REMPI spectra of $H_2(X, v_x=0)$[18,19] suggest that the two-photon excitation cross sections are dependent on J. We have estimated the rotational temperature in the 0-0, 0-2, 9-7, and 5-8 bands, neglecting variations in the quantities listed above. All of the results fall in the range 200-600 K, with all but one temperature clustered around 350 K. The Boltzmann plots were not very straight, producing standard deviations of about 25% on the temperatures. However, we conclude that the rotational temperature is well below both the temperature of

the Ta wire (about 2000 K) and the effective vibrational temperature, consistent with the results of Hall et al.

In summary, we have detected H_2 in ground electronic state vibrational levels v_X=0, 2, and 4 to 11 by 2+1 REMPI. This was the first detection of H_2 ($v_X \geq 6$) by optical means. We are capable of detecting densities of $H_2(v_X=9)$ as low as 10^7 cm^{-3}. Rotational temperatures of these bands were considerably lower than either the Ta wire temperature or the effective vibrational temperature.

ACKNOWLEDGEMENT

This work was sponsored by the Air Force Office of Scientific Research. We thank Mark J. Dyer for construction of part of the apparatus and James R. Peterson for extensive discussions.

REFERENCES

1. K. N. Leung and W. B. Kunkel, Phys. Rev. Lett. **59**, 787 (1987).
2. J. R. Hiskes, Comments At. Mol. Phys. **19**, 59 (1987).
3. M. Pealat, J.P.E. Taran, J. Taillet, M. Bacal, and A. M. Bruneteau, J. Appl. Phys. **52**, 2687 (1981).
4. P. J. Eenshuistra, J.H.M. Bonnie, J. Los, and H. J. Hopman, Phys. Rev. Lett. **60**, 341 (1988).
5. G. C. Stutzin, A. J. Young, A. S. Schlachter, K. N Leung, and W. B. Kunkel, Chem. Phys. Lett. **155**, 475 (1989).
6. E. E. Eyler, J. Gilligan, E. McCormack, A. Nussenzweig, and E. Pollack, Phys. Rev. A **36**, 3486 (1987).
7. D.A.V. Kliner, K.-D. Rinnen, and R. N. Zare, J. Chem. Phys. **90**, 4625 (1989).
8. R. I. Hall, I. Cadez, M. Landau, F. Pichou, and C. Schermann, Phys. Rev. Lett. **60**, 337 (1988).
9. S. T. Pratt, P. M. Dehmer, and J. L. Dehmer, J. Chem. Phys. **78**, 4315 (1983).
10. S. T. Pratt, P. M. Dehmer, and J. L. Dehmer, Chem. Phys. Lett. **105**, 28 (1984).
11. S. T. Pratt, P. M. Dehmer, and J. L. Dehmer, J. Chem. Phys. **86**, 1727 (1987). Phys. Rev. A **39**, 3932 (1989).
12. I. Dabrowski, Can. J. Phys. **62**, 1639 (1984).
13. P. Senn and K. Dressler, J. Chem. Phys. **87**, 6908 (1987).
14. A. Monfils, J. Mol. Spectrosc. **15**, 265 (1965).
15. T. Namioka, J. Chem. Phys. **40**, 3154 (1964).
16. J. D. Buck, D. C. Robie, A. P. Hickman, D. J. Bamford, and W. K. Bischel, Phys. Rev. A **39**, 3932 (1989).
17. W. Huo, personal communication, 1989.
18. E. E. Marinero, C. T. Rettner, and R. N. Zare, Phys. Rev. Lett. **48**, 1323 (1982).
19. E. E. Marinero, R. Vasudev, and R. N. Zare, J. Chem. Phys. **78**, 692 (1983).

Table I. EF-X bands observed by 2+1 REMPI. Bands for which the Q1 line was observed are marked with an X. Bands within the spectral region scanned whose Q1 lines were unobstructed but not observed are marked with an O.

v_X	0	1	2	3	4	5	6	7	8	9	10	11	12	13	14
v_{EF}															
0	X		X			X	O								
1	O	O				O			X	X					
2							X		X	X					
3					X		X		X	X	O				
4							O	O	X	X	O				
5				O				X	X	X					
6	X	O	X					X	X	X		O			
7								O	X	X		O			
8						O		X	X	X					
9								X	X		O		O		
10									O	X		O		O	O
11										O	X	O			O
12			O	O			O		X	O				O	O
13										O	O	X	O		O
14											O	X	O		
15						O				O	O	O		O	O
16										O		O			O
17				O	O						X				
18											O	O	O	O	O
19											O	O		O	O
20												O	O	O	
v_{GK}															
0												O	O		
1													O		

FIGURE CAPTIONS

Figure 1. Apparatus diagram.

Figure 2. 2+1 EF-X REMPI spectrum of vibrationally excited H_2. All identified lines are in Q-branches, unless otherwise marked.

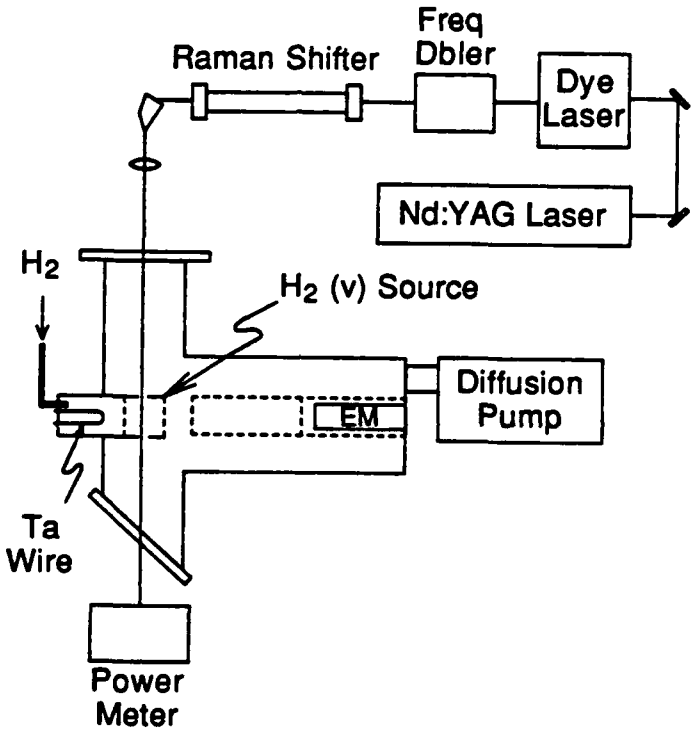
Freq
Dbler
Raman Shifter
Dye
Laser
Nd:YAG Laser
H2
H2 (v) Source
Diffusion
Pump
EM
Ta
Wire
Power
Meter
RA-2599-13

Figure 1

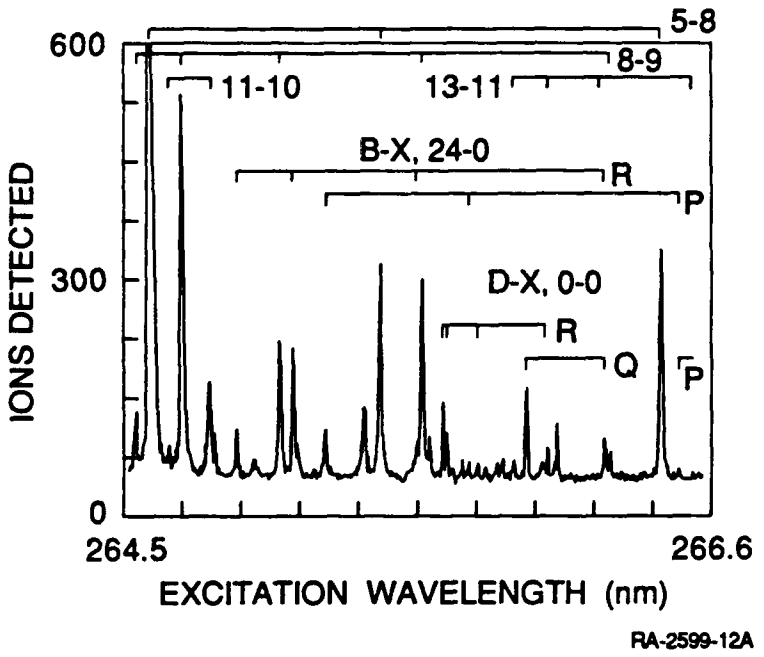
5-8
600
8-9
11-10
13-11
B-X, 24-0
R
P
300
D-X, 0-0
R
Q
P
0
IONS DETECTED
264.5
266.6
EXCITATION WAVELENGTH (nm)
RA-2599-12A

Figure 2

Appendix D

CALCULATION OF TWO-PHOTON PHOTOABSORPTION CROSS SECTIONS FOR X→ E, F TRANSITIONS FROM $H_2(v)$

CALCULATION OF TWO-PHOTON PHOTOABSORPTION CROSS SECTIONS FOR X → E, F TRANSITIONS FROM $H_2(v)$

To determine vibrational temperatures from two-photon spectra (either REMPI or LIF), we need to know the two-photon excitation cross section for the relevant line. Because of the difficulties of measuring multiphoton cross sections accurately, few are available. We published our measurement of the two-photon cross section for excitation in the Q(1) line of the 6-0 band from the X state to the EF state (Appendix A). Our measurement agreed reasonably well with the theoretical calculation of this cross section. Measurements of cross sections for excitation from higher vibrational levels using the same technique will be difficult, because the population of the lower level must be known. (We believe we have a method for accomplishing this task, however, on the basis of saturation of the excitation.)

In lieu of measured cross sections, we to asked Dr. Winifred Huo of NASA Ames Research Center, who had calculated the absolute two-photon cross section we measured (Appendix A), to calculate the two-photon cross sections for the Q(J) for J = 0 and 1 lines in all the bands that we might reasonably expect to cover, originating from vibrationally excited levels in the X state. She recently completed the calculation, including all the bands originating from V" = 0 to 14 in the X state and terminating at v' = 0 to 14 in the EF state. Because this work has not yet been published, it will be described here in more detail.

The procedure is similar to that of Huo and Jaffe.[1] Electronic wavefunctions were calculated at the nearly full configuration interaction (CI) level using a Slater basis set of 20, 14 π functions. Vibrational wavefunctions in all relevant states were obtained from numerical solutions of the one-dimensional Schrodinger equation. The potential energies used for the X $^1\Sigma_g^+$ and EF $^1\Sigma_g^+$ states were taken from Kolos and Wolniewicz[2] and Wolniewicz and Dressler.[3] Two approaches were used in the treatment of the potentials of the intermediate states.

The potential energies of the B $^1\Sigma_u^+$ and C $^1\Pi_u$ states were obtained from Wolniewicz and Dressler[3] and Kolos and Wolniewicz,[4] supplemented at large internuclear distances by CI results from Huo and Jaffe.[1] The potentials for the B' $^1\Sigma_u^+$ and D $^1\Pi_u$ states were taken from a Rydberg-Klein-Rees analysis of spectroscopic data by Sharp,[5] also supplemented at large internuclear distance by results from Huo and Jaffe.[1] Contributions to the two-photon amplitudes from the higher states were smaller. Vibrational wavefunctions of the intermediate states were neglected so that contributions of the higher states could be estimated.

Amplitudes were evaluated using only the electronic wavefunctions at each internuclear distance, then integrated over the vibrational wavefunctions of the X and EF states. The photon-energy dependence of these higher states' contributions was determined for the EF (v' = 6) - X (v" = 0) transition only; the energy transition amplitudes were guaranteed by forcing the vibronic wavefunctions to satisfy the off-diagonal S(0) and S(-1) sum rules described by Huo and Jaffe[1] and Dalgarno and Epstein.[6]

The calculated cross sections for the Q(1) lines are shown in Table 1. We detected many of these lines in our two-photon MPI spectra of vibrationally excited H_2. Although our experimental data contained contributions from other J levels, we limited our identification and verification efforts to J = 1 lines to maximize our efficiency of comparison with the calculations. The Q(1) lines we detected are underlined in Table 1; the lines that were in our tuning range but not observed are in parentheses. The lines separate the bands according to the Raman order used for the generation of laser radiation for the detection. This is an indication of the laser power available for excitation, which decreases exponentially with increasing order. The correlation between the magnitudes of the cross sections and the observations is good, taking into account pulse power and level population. All the bands originating from a given v" with cross sections above the smallest one for an observed band are also expected to be observed. These characteristics hold for almost all the observations.

The v" = 6 $\rightarrow$ v' = 2 band is anomalous: the calculated cross section predicts nonobservability. Although the predicted locations of this line agreed very well with its location, there is always the possibility of an error. Otherwise the explanation must lie in some unpredicted perturbation. Other than that one line, only bands originating from v'= 10 and 11, which are more subject to theoretical error, fail to show the expected pattern. It would be interesting to measure the cross sections for the anomalous bands to reconcile the experimental observations and theoretical calculations.

Table I

TWO-PHOTON ABSORPTION CROSS SECTIONS FOR THE Q_1 LINES
OF THE $H_2\, X^1\Sigma_g^+$ (v") $\rightarrow$EF $^1\Sigma_g^+$ (v') TRANSITIONS

Calculated by W. Huo, in units of 10^{-36} cm^4

v"-X	0	1	2	3	4	5	6	7
v'-EF								
0	4.86	12.8	13.1	6.72	1.82	0.257	(0.178)	6.55E-4
1	(4.8E-6)	(1.0E-04)	4.2E-6	4.9E-5	1.6E-6	(4.80E-5)	3.6E-04	0.0044
2	0.0027	0.0011	6.7E-04	2.0E-4	0.0016	9.02E-4	8.6E-04	0.0322
3	6.70	6.09	8.19	9.92	8.94	6.50	4.77	3.96
4	0.0253	0.0124	0.0054	0.0463	0.0425	0.0612	(0.0103)	(0.129)
5	0.0300	0.00413	0.0213	(0.032)	6.1E-05	0.0777	0.295	0.774
6	3.61	(0.0660)	3.31	1.55	2.07	12.2	13.0	6.99
7	1.19	0.00321	1.16	0.290	1.09	3.54	1.70	(0.0026)
8	0.703	0.021	0.70	4.59E-4	1.12	(0.681)	0.38	4.36
9	1.67	0.197	1.49	0.165	2.75	0.112	4.68	10.8
10	1.38	0.319	1.04	0.481	1.85	0.206	5.37	3.44
11	0.975	0.415	0.518	0.741	0.757	0.983	2.93	0.00504
12	0.928	0.591	(0.307)	(1.10)	0.250	1.83	(1.04)	1.99
13	0.791	0.729	0.113	1.23	0.00923	2.02	0.0387	4.17
14	0.620	0.761	0.0161	1.10	0.0656	1.56	0.244	3.58

Table I (continued)

v'-X	8	9	10	11	12	13	14
v'-EF							
0	4.2E-5	1.5E-6	6.4E-6	2.4E-6	5.4E-6	8.3E-7	9.1E-8
1	0.0293	0.248	1.74	7.79	17.9	10.5	0.179
2	0.214	1.09	4.53	8.60	1.65	10.8	3.92
3	3.46	3.06	(2.76)	2.57	2.34	2.26	2.36
4	0.705	2.80	(6.57)	4.89	0.219	1.24	41.2
5	2.17	5.17	6.47	0.968	2.46	0.426	5.85
6	3.28	1.53	0.178	(0.394)	0.316	0.383	0.144
7	1.87	5.02	3.88	(0.0013)	2.36	0.370	35.4
8	7.79	5.91	0.537	1.86	0.621	1.29	2.01
9	5.68	0.170	(1.70)	1.18	(0.750)	0.113	7.95
10	(0.125)	3.95	1.97	(0.632)	1.02	(0.914)	(0.0445)
11	4.73	(4.39)	0.0198	(2.46)	0.0551	0.585	(1.28)
12	6.41	(0.575)	2.28	0.783	1.39	(0.0467)	(1.28)
13	2.57	(0.963)	(2.90)	0.254	(1.04)	0.893	(0.0077)
14	0.0262	3.84	(0.590)	1.99	(0.0030)	0.667	5.80

REFERENCES

1. W. M. Huo and R. L. Jaffe, Chem. Phys. Lett. **101**, 463 (1983).
2. W. Kolos and L. Wolniewicz, J. Chem. Phys. **43**, 2429 (1965).
3. L. Wolniewicz and K. Dressler, J. Mol. Spectrosc. **67**, 416 (1977).
4. W. Kolos and L. Wolniewicz, J. Chem. Phys. **48**, 3672 (1968).
5. T. E. Sharp, Atomic and Nuclear Data Tables **2**, 119 (1971).
6. A. Dalgarno and S. T. Epstein, J. Chem. Phys. **50**, 2837 (1969).

Appendix E

STIMULATED-EMISSION PUMPING OF HYDROGEN

STIMULATED-EMISSION PUMPING OF HYDROGEN

In our efforts to make a source of highly vibrationally excited H_2, we explored a technique based on stimulated-emission pumping of H_2 through the EF state. We were unable to detect any vibrationally excited H_2 $X^1\Sigma_g^+$ in these experiments and so turned to the approach described in Appendix C. However, the results of these experiments were quite interesting, and we believe this is potentially a powerful method for studying the dynamics of highly vibrationally excited H_2. Further experiments using this technique are currently being planned, and proposals for them will be submitted in the future. Here we will describe the experiments we performed, explain why we believe vibrationally excited H_2 X was not observed, and suggest ways to overcome the problems.

Stimulated emission in the ir EF-B bands and vacuum uv B-X and C-X bands after population of the EF(v = 6) level by two-photon absorption from an ArF laser beam was first observed in 1983 by the Rhodes group at the University of Illinois at Chicago.[1] The laser system they used for excitation was a special device, producing 20 mJ in 10-ps pulses. However, in 1988, Dr. H. F. Döbele and coworkers at the University of Essen[2] observed stimulated emission in both EF-B and B-X bands using a commercial narrow-band ArF laser of the same make as ours. When we learned of this development at a seminar given by Dr. Döbele at SRI, we perceived the possibility of using this technique to create highly vibrationally excited H_2 $^1\Sigma_g^+$ because B $\rightarrow$ X transitions favor those to high v" final states. We quickly set up an experiment and immediately observed stimulated emission in the EF-B bands. From the intensity of the EF-B emission, we estimated that 4% of the H_2 (X) was being pumped through the EF-B transition. To obtain a flux of red photons high enough to stimulate the EF-B transition, we had to use a high pressure of H_2; the maximum pumping rate occurred at 300 torr of H_2. This result implies that a high density of H_2 was passing through the B state. We did not look for stimulated emission in the vacuum ultraviolet. However, H_2 in the B state fluoresces quickly so that quenching is not significant, even at this pressure. We expected, therefore, that even if the B-X transition did not become stimulated, a substantial density of H_2 would radiate into the high vibrational levels of the X state.

There has been an intensive effort to discover the rates for collisional relaxation from high vibrational levels of H_2 (X). Measurements[3] have not extended above v = 2, but extensive theoretical calculations have been done.[4] From those calculations, we estimated that a substantial population of H_2 (v = 8) should have been created, with a decay time of about 30 ns. Considering the large density of H_2 (v = 8) created, we expected to be able to detect this level using two-photon LIF through the EF state. Furthermore, we expected that most of the vibrationally excited H_2

would cascade down through the vibrational levels via V-T relaxation, so that at longer time scales it would be possible to observe populations in each of the levels down to v = 1. We were, however, unable to detect any vibrationally excited H_2 in the X state. Next we explored the possibility that the excited population was lost by V-T relaxation by the H_2 gas. We therefore ran the experiment at H_2 pressures down from 500 torr to 500 mtorr but still observed no excited state population.

After an analysis of the experiments described alone, it now seems likely that the main fault in the low-pressure experiments was an extensive depletion of the EF population by photoexcitation of the EF state to higher levels, because at low pressures the flux of red photons from the EF-B bands is not enough to make stimulated emission competitive with ionization. This problem could be remedied by supplying red photons with a laser, tuned to either 750 or 830 nm. (This tuning range is available from dye lasers and also from the new Ti:sapphire lasers.) The excitation cross section was measured during this project; it is 6×10^{-18} cm_2 at 193 nm. With an ArF laser pulse energy of 50 mJ, the rate of excitation is then 4×10^{10} S^{-1}. The integrated stimulated-emission cross section for the EF-B transition can be obtained from the known transition moment;[6] it is 1.4 × 10-3 cm^2 Hz. If we assume the lines are Doppler-broadened, the spectral cross section for stimulated emission is 4.4×10^{-13} cm^2. This photon flux at 830 nm required for stimulated emission to match excitation is 9×10^{22} cm^{-2} s^{-1}. A typical dye laser, producing 10 mJ at 830 nm in a 3-mm-diameter pulse of 10 ns duration, has a photon flux of 6×10^{25} cm^2 s^{-1}, easily enough to stimulate the downward transition to the B state and thus overcome the upward excitation loss.

In the high pressure experiments, it is likely that the main problem was 2+1 multiphoton ionization of the H_2 (X, v = 8) by the probe laser used to produce LIF. It might be possible to overcome this problem simply by using a less tightly focused probe laser. It is difficult to detect ions in this experiment, because many are formed by the excimer laser pulse; but it might be possible to detect those ions also.

REFERENCES

1 H. Pummer, H. Egger, T. S. Luk, T. Srinivasan, and C. K. Rhodes, "Vacuum-ultraviolet stimulated emission from two-photon-excited molecular hydrogen", Phys. Rev. A **28**, 795 (1983).

2. U. Czarnetski, H. F. Döbele, and B. Ruckle, "Stimulated IR- and vacuum-UV emission following two-photon-excitation of molecular hydrogen using an ArF laser," Appl. Phys. B **48**, 37 (1989).

3. T. G. Kreutz, J. Gelfand, R. B. Miles, and H. Rabitz, "A time domain photoacoustic study of the collisional relaxation of vibrationally excited H_2", Chem. Phys. **124**:359 (1988).

4. M. Cacciatore, M. Capitelli, and M. Dilonardo, "A joint vibroelectronic mechanism in the dissociation of molecular hydrogen in nonequilibrium plasmas", Chem. Phys. **34**, 193 (1978).

5. Glass-Maujean, P. Quadrelli, and K. Dressler, "Transition moments, eigenvectors, and transition probabilities for H_2", Atomic Data and Nuclear Data Tables **30**, 274 (1984).

6. M. Cacciatore, M. Capitelli, and M. Dilonardo, "A joint vibroelectronic mechanism in the dissociation of molecular hydrogen in nonequilibrium plasmas", Chem. Phys. **34**, 193 (1978).

Appendix F

LASER-BASED DETECTION OF HIGHLY VIBRATIONALLY EXCITED H_2 FOR PLASMA DIAGNOSTICS

Reprinted from SPIE Vol. 1061—Microwave and Particle Beam Sources and Directed Energy Concepts

Laser-based detection of highly vibrationally excited H_2 for plasma diagnostics

Daniel C. Robie, L.E. Jusinski, and William K. Bischel

Molecular Physics Laboratory, SRI International
333 Ravenswood Avenue, Menlo Park, CA 94025

ABSTRACT

It has been suggested that the main source of H^- in hydrogen plasmas is dissociative attachment to $H_2(v\geq4)$. In order to test models that include this process, it is necessary to measure the populations of the relevant vibrational levels inside the plasma. We have constructed a source of vibrationally excited H_2 using a recently discovered hot-wire effect. Using 2+1 resonantly enhanced multiphoton ionization (REMPI) through the EF state, we have detected H_2 in 27 bands from X(v"=4-11) to EF(v'=0-14). Rotational temperatures appear to be 300-800 K, well below that required for thermal excitation of the observed vibrational levels. The population of vibrational levels appears to fall off dramatically between v"=9 and 10.

1. INTRODUCTION

The main source of H^- in hydrogen plasmas is believed to be dissociative attachment to vibrationally excited $H_2(X^1\Sigma_g^+)$.[1,2] To examine this, it is necessary to measure the populations of high vibrational levels of $H_2(X^1\Sigma_g^+)$ inside the plasma. In the course of developing a technique to do this, we have constructed a source of highly vibrationally excited H_2. Using 2+1 REMPI, via vibrational levels of the $EF^1\Sigma_g^+$ state, we have already detected $H_2(X, v" = 4\text{-}11)$.[3] This is the first report of the detection of H_2 (X, v" > 5) by optical means.

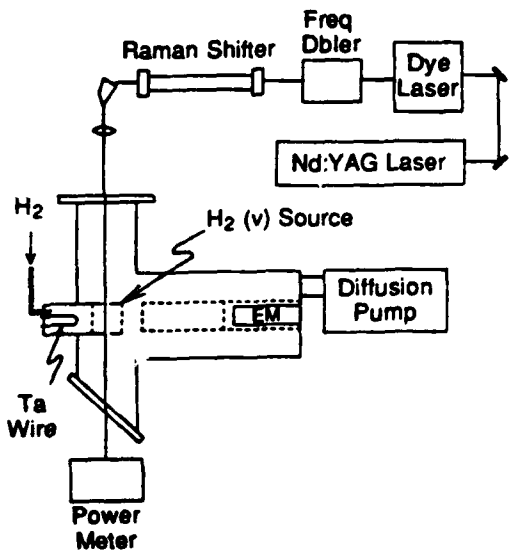

Figure 1. Apparatus diagram.

2. EXPERIMENTAL

Vibrationally excited H_2 was generated using a hot-wire effect discovered recently by Hall et al.[4] and Eenshuistra et al.[5] The apparatus is diagrammed in Figure 1. A tantalum wire 23 cm long (initially .38 mm in diameter) was heated with 7.5 A of dc current at 20 V. The wire was enclosed in a water-cooled stainless steel cylinder 15 cm long and 2.5 cm in diameter. H_2 flowed slowly into the cylinder at the base of the wire. The pressure in the cylinder was 10 mtorr. At the end of the cylinder, a quartz cylinder 1.5 cm long was attached, with grids at both ends. The laser beam passed through the quartz cylinder via two 1/8"-diameter holes drilled in the sides. Surrounding the quartz cylinder was a diffusion-pumped chamber. When the pressure in the cylinder was 10 mtorr, the pressure in the chamber was 100 μtorr. Coaxial with the cylinder was a drift tube, ending with an EMI 9642 B electron multiplier. The electron multiplier cathode, the drift tube, and the two grids attached to the quartz cylinder were all connected to high voltage supplies. Potentials were adjusted to give the best mass resolution and narrowest peaks for H^+ and H_2^+ ions. Typical voltages were 0 V, -100 V, -500 V, and - 2500 V, from the first grid to the cathode. Signals from

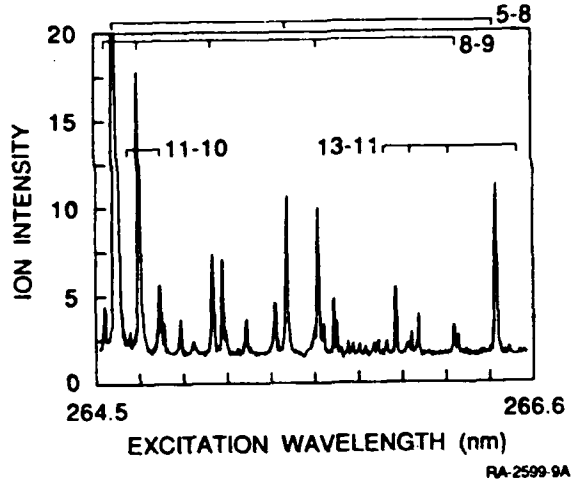

Figure 2. 2+1 EF←X REMPI spectrum of vibrationally excited H_2. All identified lines are in Q-branches. Line assignments for the EF←X bands are from Dabrowski[11] and Senn and Dressler.[12]

v_X	4	5	6	7	8	9	10	11	12
v_{EF}									
0		X		O	O				
1		O	O	O	X	X			
2			O		X	X			
3	X		X		X	X	O		
4			O		X	X	O		
5				X	X	X	O		
6				X		X	O	O	
7				X		X	O	O	
8		O		X	X	X	O	O	O
9				X	X		O	O	O
10							X	O	O
11							X	O	O
12			O			O		O	O
13						O		X	O
14						O		X	O

Table 1. EF←X bands observed by 2+1 REMPI. Observed bands are indicated by an X. Bands within the spectral region scanned that were not observed are indicated by an O.

the electron multiplier were amplified and peaks of masses 1 and 2 amu were followed separately with boxc ar averagesTunable laser light was generated by a doubled dye laser, pumped by a Nd:YAG laser producing either 355 nm or 532 nm light. The tuning range of the doubled dye laser was extended with an H_2 Raman shifter. The desired wavelength was selected with a crystalline quartz or Homosil Pellin-Broca prism, and focused with lenses of 20 to 100 cm focal length into the center of the quartz cylinder. Scans over most of the spectral region between 230 nm and 285 nm were performed.

3. RESULTS

At the blue end of the scanned region, the spectrum is relatively simple, composed only of bands originating from $H_2(X,v'' \leq 7)$. At the red end there is substantial congestion from 3+1 MPI bands, originating from $H_2(X, v'' = 0)$ and resonant with the B, B', C, and D states.[6-8] (We have also detected strong 3+1 REMPI lines in the H Lyman progression from 285 nm to 274 nm for excitation to n = 5 to 12.) Figure 2 shows a part of the H^+ spectrum, from 264.5 to 266.6 nm, including the 5-8, 8-9, 11-10, and 13-11 bands. The H^+ spectrum is richer and more intense than the H_2^+ spectrum in this wavelength region. Table 1 shows all the 2+1 bands observed (marked with an X) and all the bands lying within the spectral region scanned that were not observed (marked with an O). For $v'' \leq 6$, only bands terminating at inner-well E state vibrational levels ($v' = 0, 3$ or 6) were observed. For $7 \leq v'' \leq 9$, bands terminating at EF levels that are primarily E-state ($v' = 3,6,9$), and primarily F state ($v' = 1,2,4,5,7, 8$) were both observed. Finally, for $v'' \geq 10$ pairs of bands terminating at adjacent large v' were observed. This pattern is likely to be primarily due to variations in the overlap of the vibrational wavefunctions of the X and EF states.

The two-photon absorption cross section for the EF←X transition has been measured and calculated[9] for the 6-0 band. Experiments and theory agree quite well. However, cross sections for hot bands have not yet been measured or calculated. Assuming that the two-photon excitation cross sections, the excited state absorption cross section and the branching ratio for H^+ production after absorption are the same for all the rotational lines within a given band, a rotational temperature can be found from a Boltzmann plot. The resulting temperatures range from 300 to 800 K. A strong dependence of the cross sections and branching ratios on the rotational energy is necessary to raise the estimated rotational temperature to near the temperature of the Ta wire (about 2000 K) or to the effective vibrational temperature. This is unlikely. A rotational temperature well below the other two temperatures is consistent with earlier findings.[4,10]

In order to deduce the vibrational level populations, it is necessary to know the cross sections and branching ratios referred to above. Lacking these, we have estimated vibrational level populations from band intensities. Qualitatively, the strongest bands originating from v" = 10 and 11 are considerably weaker than the strongest band originating from v" = 9. Hall et al.[4] reported that populations in $6 \leq v'' \leq 9$ dropped by a factor of about three for each increase in the vibrational quantum number of one. (Since their detections ystem was tuned for H^- ions with no kinetic energy, they could not detect any level higher than v" = 9.) Our observations are qualitatively in accord with theirs for $v'' \leq 9$. However, we observed that the vibrational level population drops off considerably more dramatically between v" = 9 and v" = 10. This could be because of an increased electron attachment rate. We have not measured the electron density in the source, but the dc polarity of the Ta wire with respect to the case did not affect the spectra; neither did striking a discharge in the source. However, there is likely to be some thermionic emission, limited by space charge effects. It is also possible that the production mechanism for the vibrationally excited H_2 favors the production of $H_2(X, v'' \leq 9)$.

The number of ions detected can be estimated from known apparatus parameters. We estimate the density of H_2 (X, v" = 9) to be $\approx 10^9$ cm^{-3}. This is consistent with Hall et al.[4] who estimated the density of $H_2(X, v'' = 9)$ to be 3×10^9 cm^{-3} in a similar source.

4. CONCLUSION

In summary, we have detected by 2+1 REMPI H_2 in X-state vibrational levels from v" = 4 to 11. The source was a hot Ta wire in a stainless steel cylinder with 10 mtorr H_2 flowing slowly. The rotational temperature was considerably less than either the wire temperature or the effective vibrational temperature. The vibrational level population dropped off dramatically between v" = 9 and 10.

Using this source, we will measure two-photon excitation cross sections for the EF $^1\Sigma_g^+ \leftarrow X^1\Sigma_g^+$ transition. We will then be able to assess the comparative merits of remote detection of vibrationally excited H_2 by laser-induced fluorescence, detecting either infrared emission in the EF→B bands, or vacuum UV emission in the B→X bands.

5. ACKNOWLEDGEMENT

This work was sponsored by the Air Force Office of Scientific Research. We thank James R. Peterson for alerting us to the work of Refs. 4 and 5 and Mark J. Dyer for construction of part of the apparatus.

6. REFERENCES

1. K. N. Leung and W. B. Kunkel, "H^- formation process in a multicusp ion source," Phys. Rev. Lett. 59, 787 (1987).

2. J. R. Hiskes, "Atomic processes in hydrogen negative ion discharges," Comments At. Mol. Phys. 19, 59 (1987).

3. D. C. Robie, L. E. Jusinski, and W. K. Bischel, "Generation of H_2(v=0 to 2 and 4 to 11) and detection of 2+1 resonantly enhanced multiphoton ionization," submitted for publication, 1988.

4. R. I. Hall, I. Cadez, M. Landau, F. Pichou, and C. Shermann, "Vibrational excitation of hydrogen via recombinative desorption of atomic hydrogen gas on a metal surface," Phys. Rev. Lett. 60, 337 (1988).

5. P. J. Eenshuistra, J.H.M. Bonnie, J. Los, and H. J. Hopman, "Observation of exceptionally high vibrational excitation of hydrogen molecules formed by wall recombination," Phys. Rev. Lett. 60, 341 (1988).

6. S. J. Pratt, P. M. Dehmer, and J. L. Dehmer, "Photoionization of excited molecular states. H_2 $C^1\Pi_u$"," Chem. Phys. Lett. 105, 28 (1984).

7. S. J. Pratt, P. M. Dehmer, and J. L. Dehmer, "Resonant multiphoton ionization of H_2 via the $B'^1\Sigma_u^+$, v=7, J = 2 and 4 levels with photoelectron energy analysis," J. Chem. Phys. 78, 4315 (1983).

8. S. J. Pratt, P. M. Dehmer, and J. L. Dehmer, "Photoelectron studies of resonantly enhanced multiphoton ionization of H_2 via the $B'\ ^1\Sigma_u^+$ and the $D\ ^1\Pi_u$ states," J. Chem. Phys. 86, 1727 (1987).

9. J. D. Buck, D. C. Robie, A. P. Hickman, D. J. Bamford, and W. K. Bischel, "Two-photon excitation and excited state absorption cross sections for H_2 $EF\ ^1\Sigma_g^+$ (v=6): measurement and calculations," submitted for publication, 1988.

10. J.H.M. Bonnie, "Multiphoton ionization for hydrogen plasma diagnostics," Ph.D. thesis, Universiteit van Amsterdam, 1987, p.76.

11. I. Dabrowski, "The Lyman and Werner bands of H_2," Can. J. Phys. 62, 1639 (1984).

12. P. Senn and K. Dressler, "Spectroscopic identification of rovibronic levels lying above the potential barrier of the $EF\ ^1\Sigma_g^+$ double-minimum state of the H_2 molecule," J. Chem. Phys. 87, 6908 (1987).